Distinct release properties of glutamate/GABA co-transmission serve as a frequency-dependent filtering of supramammillary inputs

Himawari Hirai[1], Kohtarou Konno[2], Miwako Yamasaki[2], Masahiko Watanabe[2], Takeshi Sakaba[1], Yuki Hashimotodani[1*]

[1]Graduate School of Brain Science, Doshisha University, Kyoto 610-0394, Japan
[2]Department of Anatomy, Faculty of Medicine, Hokkaido University, Sapporo, Japan

*To whom correspondence should be addressed:
Yuki Hashimotodani, PhD
Graduate School of Brain Science
Doshisha University
1-3 Tatara Miyakodani, Kyotanabe, Kyoto
610-0394, Japan
Phone: +81-774-65-6057
E-mail: hashimotodani@gmail.com

Abstract

Glutamate and GABA co-transmitting neurons exist in several brain regions; however, the mechanism by which these two neurotransmitters are co-released from the same synaptic terminals remains unclear. Here, we show that the supramammillary nucleus (SuM) to dentate granule cell synapses, which co-release glutamate and GABA, exhibit differences between glutamate and GABA release properties in paired-pulse ratio, Ca^{2+}-sensitivity, presynaptic receptor modulation, and Ca^{2+} channel-vesicle coupling configuration. Moreover, uniquantal synaptic responses show independent glutamatergic and GABAergic responses. Morphological analysis reveals that most SuM boutons form distinct glutamatergic and GABAergic synapses in proximity, each characterized by GluN1 and $GABA_A\alpha1$ labeling, respectively. Notably, glutamate/GABA co-transmission exhibits distinct short-term plasticities, with frequency-dependent depression of glutamate and frequency-independent stable depression of GABA. Our findings suggest that glutamate and GABA are co-released from different synaptic vesicles within the SuM terminals, and reveal that distinct transmission modes of glutamate/GABA co-release serve as frequency-dependent filters of SuM inputs.

Introduction

Despite the classical view of Dale's Principle known as "one neuron, one transmitter": a single neuron releases a single neurotransmitter (Eccles et al., 1954), a growing body of evidence has demonstrated that many types of neurons in several brain regions co-release multiple neurotransmitters including classical neurotransmitters (glutamate, GABA, glycine, and acetylcholine), monoamines, purins, and neuropeptides (Hnasko and Edwards, 2012; Vaaga et al., 2014; Trudeau and El Mestikawy, 2018; Wallace and Sabatini, 2023). While this co-release is thought to contribute to several brain functions (Nusbaum et al., 2001; Trudeau et al., 2014; Tritsch et al., 2016; Ma et al., 2018; Kim and Sabatini, 2023), little is known about the functional implications of the co-release of two or more neurotransmitters into neural circuits and the molecular mechanisms of how multiple neurotransmitters are co-transmitted. Here, we define co-release as the release of multiple neurotransmitters from a single neuron, regardless of whether the neurotransmitters are packaged in the same or different synaptic vesicles, and co-transmission as synaptic transmission occurring by multiple neurotransmitters and detected by distinct postsynaptic receptors (Wallace and Sabatini, 2023).

The co-release of glutamate and GABA, both fast-acting and functionally opposing neurotransmitters, has recently been identified in several brain regions of the adult brain (Trudeau and El Mestikawy, 2018; Kim and Sabatini, 2023; Wallace and Sabatini, 2023). In particular, the lateral habenula and dentate gyrus (DG) of the hippocampus have been extensively studied for the co-release of glutamate and GABA. The lateral habenula neurons receive glutamate/GABA co-releasing synaptic inputs from the entopeduncular nucleus (EP) (Shabel et al., 2014; Wallace et al., 2017; Root et al., 2018) and ventral tegmental area (VTA) (Root et al., 2014; Yoo et al., 2016; Root et al., 2018). Hypothalamic supramammillary nucleus (SuM) neurons projecting to the DG also co-release glutamate and GABA (Pedersen et al., 2017; Hashimotodani et al., 2018; Billwiller et al., 2020; Chen et al., 2020; Li et al., 2020; Ajibola et al., 2021). To understand how synaptic inputs mediated by the co-release of the excitatory action of glutamate and the inhibitory action of GABA are integrated and impact postsynaptic cells, it is necessary to elucidate how glutamate and GABA are co-released from the synaptic terminals. Mechanistically, if glutamate and GABA are co-released from distinct vesicle populations, each release could be differently regulated by distinct release mechanisms. Such distinct co-release modes of glutamate and GABA are expected to implement different presynaptic plasticity, which will have diverse effects on postsynaptic neurons in response to different activity patterns. By contrast, if two

neurotransmitters are co-released from the same synaptic vesicles, both glutamate and GABA release are expected to be under the same regulation.

Whether glutamate and GABA are packaged in the same or separate vesicles remains controversial. Electrophysiological studies have demonstrated the co-packaging of glutamate and GABA in the same synaptic vesicles at EP-lateral habenular synapses (Shabel et al., 2014; Kim et al., 2022). Conversely, an immunoelectron microscopy (immuno EM) study demonstrated that glutamatergic and GABAergic vesicle populations are segregated in the axon terminals of the EP and VTA projections in the lateral habenula, and that single terminals form both excitatory and inhibitory synapses (Root et al., 2018). The same study also reported segregated vesicle populations of glutamate and GABA in the axon terminals of the SuM projections in the DG (Root et al., 2018). However, the mode of co-release of glutamate and GABA from the SuM terminals has never been functionally addressed.

In this study, we investigated the release properties of glutamate/GABA co-transmission at SuM-granule cell (GC) synapses. We demonstrate that glutamate/GABA co-transmission shows independent synaptic responses and differential short-term plasticity and that their postsynaptic targets are segregated. Our results suggest that the segregation of two different populations of transmitters makes it possible to exert short-term dynamic changes in the co-transmission balance of glutamate and GABA and modulate GC activity in a frequency-dependent manner.

Results

Glutamate/GABA co-transmission shows different release probabilities and Ca^{2+} sensitivities

To optogenetically stimulate SuM inputs in the DG, channelrhodopsin-2 (ChR2) was expressed in SuM neurons by injecting a Cre-dependent adeno-associated virus (AAV) encoding ChR2-eYFP (AAV-DIO-ChR2(H134R)-eYFP) into the lateral SuM of vesicular glutamate transporter 2 (VGluT2)-Cre mice (Hashimotodani et al., 2018; Hirai et al., 2022; Tabuchi et al., 2022) (Figures 1 A and 1B). Consistent with previous reports (Boulland et al., 2009; Soussi et al., 2010; Root et al., 2018; Billwiller et al., 2020; Ajibola et al., 2021), the vast majority of ChR2-eYFP-expressing SuM boutons in the DG co-expressed VGluT2 and vesicular GABA transporter (vesicular inhibitory amino acid transporter, VIAAT) (Figures 1C-1E). We performed whole-cell patch-clamp recordings from GCs in acute hippocampal slices and recorded optically evoked excitatory or inhibitory postsynaptic currents (EPSCs or IPSCs) at SuM-GC synapses in the presence of picrotoxin or NBQX/D-AP5, respectively. To

examine whether the co-release of glutamate and GABA exhibits the same or different release properties, we first monitored the paired-pulse ratio (PPR), an index of the change in presynaptic transmitter release (Zucker and Regehr, 2002), of glutamate/GABA co-transmission by paired stimulation (inter-stimulus interval: 100 ms). As reported previously (Hashimotodani et al., 2018; Tabuchi et al., 2022), both EPSCs and IPSCs at SuM-GC synapses exhibited paired-pulse depression (Figure 1F). Importantly, we found that PPR was significantly different between EPSCs and IPSCs; EPSCs were more depressed than IPSCs (Figure 1G) (EPSC: 0.46 ± 0.03, n = 8; IPSC: 0.6 ± 0.03, n = 8, $p < 0.01$, unpaired t test). It is possible that direct illumination of presynaptic boutons could increase transmitter release due to the broadening of the presynaptic waveform or direct influx of Ca^{2+} through ChR2 (Jackman et al., 2014; Rost et al., 2022). To avoid this possibility, we stimulated SuM axons instead of SuM terminals (Supplementary Figures 1A and 1B), and obtained similar results to terminal illumination (Supplementary Figure 1C-F). Altogether, these results suggest that the release probability differs between the co-released glutamate and GABA from SuM terminals in the DG.

Since vesicular exocytosis depends on the extracellular Ca^{2+} concentration, we next examined whether reducing the release probability by lowering the extracellular Ca^{2+} concentration could have different effects on glutamate/GABA co-transmission. Reducing extracellular Ca^{2+} concentration from 2.5 to 1 mM decreased the amplitudes of EPSCs and IPSCs (Figure 1H) (EPSC: n = 14, $p < 0.001$, paired t test; IPSC: n = 15, $p < 0.001$, paired t test). Remarkably, IPSCs decreased to a greater extent than EPSCs (Figure 1I) (EPSC: 45.1 ± 4.1% of reduction, n = 14; IPSC: 58.2 ± 2.7% of reduction, n = 15, $p < 0.01$, unpaired t test), suggesting different Ca^{2+} sensitivities for glutamate and GABA release.

Co-release of glutamate and GABA differs in presynaptic modulation and Ca^{2+} channel-vesicle coupling configuration

To further investigate whether the release properties of glutamate and GABA at SuM-GC synapses are different, we next examined whether glutamate and GABA co-release are mediated by different types of Ca^{2+} channels. We found that the application of ω-conotoxin-GVIA (ω-CgTx), an N-type Ca^{2+} channel blocker, had no effect on EPSCs or IPSCs at SuM-GC synapses (Figure 2A) (EPSC: 92.5 ± 13.8% of baseline, n = 6, p = 0.53, Wilcoxon signed-rank test; IPSC: 101.7 ± 11% of baseline, n = 6, p = 0.89, paired t test). We confirmed that ω-CgTx inhibited CA3-CA1 transmission (Supplementary Figure 2) (Wu and Saggau, 1994), suggesting that ω-CgTx we used is effective. In contrast, the application of

ω-agatoxin-IVA (ω-Aga-IVA), a P/Q-type Ca^{2+} channel blocker, suppressed both EPSCs and IPSCs to the same extent at SuM-GC synapses (Figure 2B) (EPSC: 23.5 ± 4.6% of baseline, $n = 5$, $p < 0.001$, paired t test; IPSC: 23.9 ± 1.9% of baseline, $n = 6$, $p < 0.05$, Wilcoxon signed-rank test; EPSC vs IPSC: $p = 0.92$, unpaired t test), suggesting that both glutamate and GABA release rely on P/Q-type Ca^{2+} channels at SuM-GC synapses.

If the synaptic vesicle pools for glutamate and GABA are identical, the effects of presynaptic G-protein-coupled receptor (GPCR) modulation on both transmissions are expected to be the same. We therefore examined how glutamate/GABA co-transmission is regulated by presynaptic GPCRs. We previously demonstrated that the co-transmission of glutamate and GABA at SuM-GC synapses is presynaptically suppressed by group II metabotropic glutamate receptors (mGluRs) and $GABA_B$ receptors (Hashimotodani et al., 2018). In agreement with this, application of the group II mGluR agonist DCG-IV suppressed both EPSCs and IPSCs at SuM-GC synapses (Figure 2C). Notably, DCG-IV inhibited EPSCs ($IC_{50} = 0.11$ μM) to a greater extent than it did IPSCs ($IC_{50} = 0.27$ μM) (Figure 2C) (two-way ANOVA, $F_{1,51} = 8.1$, $p < 0.01$). Similar results were found with the application of 5 μM $GABA_B$ receptor agonist baclofen, which suppressed EPSCs more than IPSCs (Figure 2D) (EPSC: 51.6 ± 2.4% inhibition, $n = 8$; IPSC: 38.6 ± 4.3% inhibition, $n = 8$, $p < 0.05$, unpaired t test). These differential inhibitory effects of GPCRs on glutamatergic and GABAergic co-transmission are contrary to the expected idea of identical vesicle pools for glutamate and GABA but favor the hypothesis of separate vesicles for glutamate and GABA.

Spatial coupling between presynaptic Ca^{2+} channels and Ca^{2+} sensors of exocytosis is an essential feature in determining the properties of neurotransmitter release, and tight or loose coupling is distinguished by using two different binding rate Ca^{2+} chelators BAPTA and EGTA (Adler et al., 1991; Eggermann et al., 2011). We examined the effects of these two Ca^{2+} chelators on the co-transmission of glutamate and GABA. We found that the bath application of BAPTA-AM suppressed both EPSCs and IPSCs to the same extent (EPSC: 63.4 ± 12.2% of baseline, $n = 7$, $p < 0.01$, paired t test; IPSC: 63.4 ± 7.8% of baseline, $n = 8$, $p < 0.001$, paired t test; EPSC vs. IPSC: $p = 0.96$, unpaired t test) (Figure 2E). In contrast, EGTA-AM suppressed EPSCs, whereas it did not affect IPSCs (EPSC: 67.4 ± 7.2% of baseline, $n = 6$, $p < 0.01$, paired t test; IPSC: 93.1 ± 9.2% of baseline, $n = 6$, $p = 0.40$, Wilcoxon signed rank test; EPSC vs. IPSC: $p < 0.05$, unpaired t test) (Figure 2E). These results indicate tighter coupling between Ca^{2+} channels and synaptic vesicles for GABA release than for glutamate release.

Minimal light stimulation of SuM inputs elicits independent EPSCs and IPSCs in GCs

We next performed minimal light stimulation to evoke a synaptic response mediated by a single vesicle release, which allowed us to detect stochastic synaptic responses of independent EPSCs and IPSCs, or compound EPSC/IPSC responses (Kim et al., 2022). In this experiment, optical stimulation was delivered in the presence of tetrodotoxin (TTX) and 4-aminopyridine (4-AP) to exclude SuM inputs-mediated polysynaptic responses, together with D-AP5 to block NMDA receptors. We also decreased the extracellular Ca^{2+} concentration to 1 mM to reduce the release probability. At intermediate holding membrane potentials (-20 to -30 mV), maximum light power illumination elicited biphasic responses (EPSC-IPSC sequence), enabling simultaneous recordings of glutamate/GABA co-transmission in GCs (Figure 3A, left). After confirming the existence of biphasic PSCs, the light power intensity was decreased to detect small synaptic events, that were stochastically observed among the 100 times stimulations (success rate = ~15%) (Figures 3A, 3B, and Supplementary Figure 3). Using this method, we analyzed 1700 trials from 17 cells and detected 86 EPSC-only, 67 IPSC-only, and 19 biphasic events (Figures 3B and 3C). These results indicate that independent EPSCs and IPSCs are the majority of synaptic responses (Figure 3D) (EPSC: 5.1 ± 0.5% probability; IPSC: 3.9 ± 0.4% probability; biphasic: 1.1 ± 0.3% probability, $n = 17$, EPSC vs bi, $p < 0.001$; IPSC vs bi, $p < 0.001$, one-way ANOVA with Tukey's *post hoc* test). To exclude the possibility that the independent EPSCs and IPSCs detected by minimal light stimulation might have masked the putative tiny synaptic responses of their counterpart currents mediated by the associated transmitters, the amplitudes and kinetics of minimal stimulation-evoked EPSCs and IPSCs were compared with or without blockers of their counterpart receptors. We found that the amplitudes and decay of minimal light stimulation-evoked EPSCs were not changed by the application of the $GABA_A$ receptor blocker picrotoxin (Supplementary Figure 4). Similarly, the amplitudes and rise time of minimal light stimulation-evoked IPSCs were not altered by application of the AMPA/kainate receptor blocker NBQX (Supplementary Figure 4). These results validate that EPSCs and IPSCs evoked by minimal optical stimulation are mediated by the stochastic release of glutamate and GABA, respectively, from single vesicles. Furthermore, by comparing minimal stimulation-evoked PSCs with strontium-induced asynchronous PSCs (see below), we found that the amplitudes of EPSCs and IPSCs evoked by minimal stimulation were identical to those of strontium-induced asynchronous EPSCs and IPSCs, respectively (Figure 3G), suggesting that PSCs evoked by minimal stimulation were mediated by a single vesicle release.

Taken together, these results indicate that glutamatergic and GABAergic co-transmission occurs independently at SuM-GC synapses.

Asynchronous release from SuM terminals exhibits independent EPSCs and IPSCs in GCs

It should be noted that minimal light stimulation of SuM inputs may elicit synchronized release of glutamate and GABA from different vesicle pools occasionally, possibly due to synchronized opening of several Ca^{2+} channels, which could be attributed to the substantial biphasic responses we detected (Figure 3D). To minimize this possibility, we recorded asynchronous quantal PSCs by substitution of extracellular Ca^{2+} with Sr^{2+}. At intermediate holding membrane potentials (-20 to -30 mV), light pulses elicited synchronized biphasic responses in the extracellular Ca^{2+} (Figure 3E). By replacing extracellular Ca^{2+} with Sr^{2+}, asynchronous quantal synaptic responses were recorded following light stimulation of the SuM inputs (Figure 3E). By repeating the light stimulation of the SuM inputs 30 times (every 10 sec), we found that the majority of asynchronous synaptic events were EPSC-only or IPSC-only, whereas biphasic PSCs represented only a minor population (Figures 3F) (EPSC: 27.9 ± 4.7 events; IPSC: 23.4 ± 4.2 events; biphasic: 2.5 ± 0.5 events, $n = 11$, EPSC vs bi, $p < 0.001$; IPSC vs bi, $p < 0.001$, one-way ANOVA with Tukey's *post hoc* test). These results further support our conclusion that glutamate/GABA co-transmission is mediated by glutamate and GABA co-released from different populations of synaptic vesicles.

Segregated glutamatergic and GABAergic postsynaptic sites at SuM-GC synapses

We then investigated whether SuM-GC synapses exhibit distinct postsynaptic sites for each neurotransmitter using immunohistochemistry. To enhance spatial resolution, we used ultrathin sections (100 nm-thick) for analysis. As shown previously (Uchigashima et al., 2011), double immunofluorescence revealed that almost all VGluT2-positive SuM terminals in the GC layer co-expressed VIAAT (Figures 4A and 4B). Further post-embedding immunogold EM (Figures 4C and 4D) showed that these terminals formed asymmetric synapse (putative excitatory) (Figure 4C) and symmetric (putative inhibitory) synapse (Figure 4D), confirming previous observations (Boulland et al., 2009; Soussi et al., 2010; Root et al., 2018). We next applied triple immunofluorescence to detect SuM terminals by VGluT2, glutamatergic postsynaptic sites by the NMDA receptor subunit GluN1, and GABAergic postsynaptic sites by the $GABA_A$ receptor subunit $GABA_A\alpha1$. In the GC layer, almost all VGluT2-positive SuM terminals were associated with GluN1 and/or $GABA_A\alpha1$

(Figures 4E and 4F). Specifically, the majority of VGluT2-positive SuM terminals were associated with both GluN1 and $GABA_A\alpha1$ (52.5%), and the remainder were associated with $GABA_A\alpha1$ (22.1%) alone or GluN1 (25.4%) alone (Figure 4G). To investigate the spatial relationship between glutamatergic and GABAergic synapses formed by individual SuM boutons, we quantified the distance between GluN1 and $GABA_A\alpha1$ cluster adjacent to the same VGluT2-positive SuM bouton. On average, the distance was 397.5 ± 8.75 nm and most SuM bouton (79.2%, 191 out of 241) form glutamatergic and GABAergic synapse within 500 nm (Figure 4H). Taken together, these results suggest that a single SuM bouton forms GluN1-containing excitatory synapse and GABAAα1-containing inhibitory synapse in separate locations, yet they remain closely proximal.

Glutamate/GABA co-transmission balance of SuM inputs is dynamically changed in a frequency-dependent manner

The results described thus far indicate that the co-transmission of glutamate and GABA is spatially segregated at SuM-GC synapses, thereby making it possible to independently regulate the co-release of glutamate and GABA from the same SuM terminals. Due to the different release properties of glutamate and GABA in the SuM terminals, glutamate/GABA co-transmission could exhibit different patterns of short-term plasticity at SuM-GC synapses. To test this possibility, we delivered a train of 10 light stimuli at 5-20 Hz, physiologically relevant frequencies (Kirk and McNaughton, 1991; Kocsis and Vertes, 1994; Ito et al., 2018; Farrell et al., 2021), to ChR2-expressing SuM inputs, and compared the short-term depression of EPSCs with that of IPSCs (Figure 5A). To exclude the putative involvement of pre- and/or postsynaptic modulations by mGluRs and $GABA_B$ receptors during a train of stimulation, pharmacologically isolated EPSCs or IPSCs were recorded in the presence of the broad-spectrum mGluR antagonist LY341495 (100 μM) and $GABA_B$ receptor antagonist CGP55845 (3 μM). We found that trains of 10 light stimuli at 5, 10, and 20 Hz elicited pronounced short-term synaptic depression of EPSCs during train with stronger depression at higher frequencies (Figures 5A and 5B). We further performed the same experiments under recording conditions with a low release probability by reducing the extracellular Ca^{2+} concentration from 2.5 to 1 mM. While train stimulation elicited a weaker depression than 2.5 mM extracellular Ca^{2+}, frequency-dependent depression was still observed (Figure 5C). In marked contrast to EPSCs, while IPSCs also exhibited short-term synaptic depression across all tested frequencies, GABAergic co-transmission showed a similar magnitude of depression across all frequencies (Figures 5D and 5E). Similarly, short-term depression of

IPSCs did not show a frequency-dependent depression with 1 mM extracellular Ca^{2+} (Figure 5F), leading to a sustained inhibitory effect at any frequency. Given that EPSCs show strong frequency-dependent depression, whereas IPSCs exhibit frequency-independent sustained depression, it is likely that the EPSC/IPSC ratio can decrease during high-frequency train stimulation. Indeed, comparing the amplitudes of the 10th EPSCs with those of the 10th IPSCs indicated that the depression of EPSCs was stronger than that of IPSCs at 10 Hz and 20 Hz (Figure 5G). We further addressed whether short-term dynamic changes in the EPSC/IPSC ratio could be observed in the same cell by recording the biphasic synaptic responses at intermediate membrane potentials that enabled simultaneous monitoring of the compound EPSC/IPSC. We found that 10 Hz train light illumination induced a stronger depression of EPSCs than of IPSCs (Supplementary Figures 5A and 5B), thereby decreasing the EPSC/IPSC ratio during the high-frequency train stimulation.

Despite the differential properties of the co-release of glutamate and GABA from SuM terminals, the difference in the magnitude of short-term depression between glutamatergic and GABAergic co-transmission could be mediated by postsynaptic mechanisms, such as AMPA receptor saturation and desensitization during burst high-frequency stimulation (Trussell et al., 1993; Brenowitz and Trussell, 2001; Heine et al., 2008). To test this possibility, we recorded EPSC trains in the presence of γ-D-glutamylglycine (γDGG), a low-affinity AMPA receptor antagonist that relieves AMPA receptor saturation and desensitization (Wadiche and Jahr, 2001; Wong et al., 2003; Foster and Regehr, 2004). As expected, 2 mM γDGG reduced the amplitude of EPSCs (60.1 ± 4.3% reduction, $n = 16$, $p < 0.001$, paired t test). Under these conditions, short-term depression with high-frequency light stimulation (10 Hz and 20 Hz) was not affected (Supplementary Figures 6A and 6B), excluding the postsynaptic contribution to the strong depression of EPSCs, suggesting that the short-term depression of EPSCs is mediated by presynaptic mechanisms. Similarly, to determine whether postsynaptic $GABA_A$ receptor saturation is involved in short-term depression during train stimulation, we used the low-affinity competitive $GABA_A$ receptor antagonist TPMPA (Sakaba, 2008; Markwardt et al., 2009; Turecek et al., 2016). We found that 300 μM TPMPA reduced the amplitude of IPSCs (47.1 ± 3.8% reduction, $n = 11$, $p < 0.01$, Wilcoxon signed rank test), while short-term depression of IPSCs in response to 10 light pulses at 10 Hz and 20 Hz did not differ before and after the application of TPMPA (Supplementary Figures 6C and 6D), excluding the involvement of $GABA_A$ receptor saturation in the short-term depression of IPSCs at SuM-GC synapses, suggesting a presynaptic origin of this short-term plasticity.

Taken together, these results suggest that SuM-GC synapses exhibit short-term dynamic changes in the glutamate/GABA co-transmission ratio during repetitive high-frequency SuM activity due to the different properties of frequency-dependent depression between glutamatergic and GABAergic transmission, favoring inhibition over excitation. Furthermore, the different properties of short-term depression of EPSCs and IPSCs also support the segregated co-transmission of glutamate and GABA at SuM-GC synapses.

SuM inputs modulate GC activity in a frequency dependent manner

We have previously demonstrated that SuM inputs associated with entorhinal cortex (EC) inputs facilitate GC firing (Hashimotodani et al., 2018). Our previous study investigated the single association of synaptic inputs, but did not examine repetitive stimulation of synaptic inputs. We investigated how the repetitive activation of SuM inputs, which implement frequency-dependent filtering of glutamatergic responses with sustained synaptic inhibition by GABAergic co-transmission, affects GC excitability. To mimic excitatory EC synaptic inputs onto GCs, a sinusoidal current was injected into the soma of GCs (Kamondi et al., 1998; Magee, 2001; Ajibola et al., 2021), which can bypass direct synaptic stimulation of the performant path (main excitatory inputs originating from EC) and, consequently, circumvent the recruitment of inhibitory circuitry. We found that a sinusoidal current at 5 Hz generated action potentials at the peak of the depolarizing phase (Figure 6A). The injected current was adjusted to generate action potentials with fewer than five spikes in each trial (10 cycles), and the optogenetically activated SuM inputs were paired at the depolarizing phase of each cycle. Paired light illumination significantly enhanced GC firing compared to sinusoidal current injections without light stimulation throughout the trial (10 stimuli) (Figures 6A and 6D). Notably, the probability of spikes further increased when GABAergic transmission was blocked by picrotoxin (Figures 6A and 6D). These results suggest that SuM inputs enhance GC firing and that GABAergic co-transmission negatively regulates the net excitatory effect of SuM inputs at 5 Hz, similar to the effects of a single associational activation of SuM and EC inputs (Hashimotodani et al., 2018). In striking contrast, at higher frequencies (10 Hz and 20 Hz), the enhancement of spike probability by SuM activation was attenuated and disappeared in the last few stimulations (Figures 6B, 6C, 6E, and 6F). Importantly, in the presence of picrotoxin, SuM activation by light stimulation enhanced GC firing, even in the last few stimulations (Figures 6B, 6C, and 6E, 6F), suggesting that SuM glutamatergic co-transmission still exerted excitatory effects in the later cycle, even during the short-term depression of glutamate release. Thus, the excitatory action of SuM inputs was filtered by the

co-released GABA during repetitive high-frequency stimulation due to frequency-independent sustained depression. These results indicate that SuM inputs modulate GC output in a frequency-dependent manner due to the different short-term plasticities of glutamate/GABA co-transmission.

Discussion

Despite evidence that glutamate and GABA are co-released from the synaptic terminals of a subset of neurons in the adult brain, whether glutamate and GABA are released from the same or distinct synaptic vesicle populations remains a debate (Shabel et al., 2014; Root et al., 2018; Kim et al., 2022). In this study, we demonstrate that the transmission properties of glutamate and GABA at SuM-GC synapses differ in PPR, Ca^{2+}-sensitivity, presynaptic GPCR regulation, and Ca^{2+} channel-synaptic vesicle coupling configuration. We further found that uniquantal synaptic responses exhibit independent EPSCs and IPSCs. The anatomical results show that the postsynaptic excitatory site (labeled by GluN1) and inhibitory site (labeled by $GABA_A\alpha1$) facing the same SuM terminals are separated with close distance. These findings provide evidence that glutamatergic and GABAergic co-transmission occurs at functionally distinct release sites (Figure 7). Owing to the functional and spatial segregation of the co-transmission of glutamate and GABA, each transmission exhibits distinct short-term plasticities, leading to different frequency-dependent effects of SuM inputs on the GC activity.

Different release properties of dual-neurotransmitter neurons have been reported in other synaptic circuits. Different PPRs (Lee et al., 2010; Silm et al., 2019; Zych and Ford, 2022) and Ca^{2+}-sensitivities (Lee et al., 2010; Zych and Ford, 2022) between co-transmission of dual-neurotransmitters are found in the retina (acetylcholine and GABA) and striatum (dopamine and glutamate or GABA). Different reliance on Ca^{2+} channels for distinct neurotransmitters have been reported in the retina (acetylcholine and GABA) (Lee et al., 2010), striatum (dopamine and glutamate) (Silm et al., 2019), and hippocampus (acetylcholine and GABA) (Takacs et al., 2018). These different release properties of the two neurotransmitters indicate a separate release from distinct vesicle pools (Lee et al., 2010; Takacs et al., 2018; Silm et al., 2019). Our study also demonstrated that glutamate and GABA co-release from SuM terminals shows differences in PPR and Ca^{2+}-sensitivity. Glutamatergic transmission exhibited a stronger depression than GABAergic transmission, suggesting that release probability of glutamate is higher than that of GABA. A higher reduction in IPSCs than EPSCs by decreasing the extracellular Ca^{2+} concentration from 2.5 to 1 mM indicates

that GABA release requires higher extracellular Ca^{2+} than glutamate release. Furthermore, using the Ca^{2+} chelators BAPTA and EGTA, we found that the spatial coupling between Ca^{2+} channels and synaptic vesicles of GABA is tighter than that of glutamate. These differences in release properties can be attributed to the different compositions of the release machinery and different spatial organizations between the release machinery and Ca^{2+} channels for glutamate and GABA release (Sudhof, 2013; Neher and Brose, 2018). Given that GABAergic co-transmission exhibits a lower release probability and a higher requirement for extracellular Ca^{2+}, together with tight coupling between Ca^{2+} channels and vesicles, synaptic vesicles for GABA release could be surrounded by a few Ca^{2+} channels in close proximity. In contrast, the synaptic vesicles for glutamate release could be surrounded by a large number of Ca^{2+} channels at longer distances than those for GABA release. As other possible mechanisms, the molecular identity and composition of the release machinery may differ between glutamate and GABA release. Future studies will have to investigate the differences in the release machinery of glutamate and GABA.

Our data showed that both glutamate and GABA release rely on P/Q-type Ca^{2+} channels at SuM-GC synapses. Interestingly, the excitatory transmission of SuM-CA2 pyramidal neuron synapses, an exclusive glutamatergic synapse (Chen et al., 2020), is also mediated by P/Q-type Ca^{2+} channels (Robert et al., 2021). Therefore, neurotransmitter release from SuM neurons depends on P/Q-type Ca^{2+} channels, irrespective of the target neurons. We found that the activation of group II mGluRs and $GABA_B$ receptors inhibited glutamatergic co-transmission more strongly than GABAergic co-transmission. Given that these GPCRs suppress presynaptic Ca^{2+} channels via $G_{i/o}$-protein, and that both transmitter releases are mediated by the same type of Ca^{2+} channels, the different extents of inhibition of the co-release of glutamate/GABA by group II mGluRs and $GABA_B$ receptors may be attributed to differential expression levels of receptors or signaling efficacy between glutamate and GABA release.

A previous EM studies reported that a single SuM terminal forms symmetric and asymmetric synapses in the DG (Boulland et al., 2009; Soussi et al., 2010; Root et al., 2018; Billwiller et al., 2020). However, confirming whether these synapses function as glutamatergic or GABAergic relies on the identification of their postsynaptic receptors, which remains unresolved. In our study, we demonstrated that both GluN1 and $GABA_A\alpha1$ were associated with common SuM boutons (Figures 4E and 4F), suggesting that these synapses represent distinct glutamatergic and GABAergic synapses. Furthermore, our analysis showed that approximately 50% of SuM boutons was associated with both GluN1

and $GABA_A\alpha1$ (Figure 4G). It should be noted, however, this percentage can be an underestimate due to the utilization of 100 nm-thick ultrathin sections, which limits the detection of co-localization events within this confined spatial range. Consequently, the actual percentage is expected to be significantly higher. Hence, the predominant synapse type of SuM boutons consists of dual glutamatergic and GABAergic synapses, with additional individual glutamatergic or GABAergic synapses.

Previous electrophysiological studies have demonstrated that both glutamate and GABA are co-packaged in the same synaptic vesicles in the lateral habenula (Shabel et al., 2014; Kim et al., 2022). Minimal optogenetic stimulation of EP terminals evoked a high proportion of biphasic PSCs over independent EPSCs and IPSCs in lateral habenular neurons, suggesting the co-release of glutamate and GABA from the same synaptic vesicles (Kim et al., 2022). While these findings seem to be contradictory with anatomical data showing distinct populations of synaptic vesicles for glutamate and GABA in the lateral habenula (Root et al., 2018), there could be technical limitations for immuno EM to examine the spatial distributions of proteins in the vesicles (Kim and Sabatini, 2023), such as interference of antibodies with each other on a tiny vesicle, limitations of antibody access to target molecules, and the stochastic nature of labeling two molecules in a single vesicle. In addition, the existence of VTA terminals, other glutamate/GABA co-release inputs (Root et al., 2014; Yoo et al., 2016; Root et al., 2018), may complicate interpretation of the co-release mechanisms in the lateral habenula. In contrast, in the DG, we found that the majority of synaptic responses evoked by both minimal light stimulation and asynchronous release at SuM-GC synapses showed independent EPSCs and IPSCs. A previous biochemical study detected VGluT2 and VIAAT in distinct purified synaptic vesicles from the hippocampus (Boulland et al., 2009). Moreover, differences in transport mechanisms between glutamatergic and GABAergic vesicles have been reported (Farsi et al., 2016). Based on this evidence, our results most likely support the hypothesis that glutamate and GABA are packaged in distinct synaptic vesicles (Figure 7). Thus, glutamate/GABA co-transmission is diverse, in that both transmitters are co-released from the same or different synaptic vesicles, depending on brain regions and synapse types.

The distinct co-transmission modes of the two transmitters have the ability to exert independent synaptic regulation compared with their co-release from identical vesicles. At SuM-GC synapses, we demonstrated that glutamatergic and GABAergic co-transmission exhibited different short-term plasticities. While glutamatergic co-transmission showed strong frequency-dependent depression, GABAergic co-transmission exhibited stable

frequency-independent depression. By this frequency-specific dynamic change of the glutamate/GABA co-transmission balance, at low-frequency burst SuM inputs, they operated as excitatory inputs, whereas at high frequency, the excitatory effects of SuM inputs on GCs were inhibited by co-transmitted GABA (Figure 6). Accordingly, GCs respond differently to SuM inputs in a frequency-dependent manner, due to the low-pass filtering of SuM-GC synapses. The fact that the theta-rhythm in the hippocampus is associated with synchronized SuM activity (Kirk and McNaughton, 1991; Kocsis and Vertes, 1994; Ito et al., 2018; Farrell et al., 2021) has important implications for the low-pass filtering of this synapse. As SuM inputs act as excitatory at 5 Hz (theta) train stimulation, but not at higher frequencies, SuM inputs may transfer their train information exclusively at the theta frequency, which could contribute to theta-mediated information processing in SuM-hippocampal circuits and their relevant brain functions, including cognitive, sleep, and navigation processes (Pedersen et al., 2017; Billwiller et al., 2020; Chen et al., 2020; Li et al., 2020; Farrell et al., 2021; Kesner et al., 2023). In addition to SuM inputs, GCs receive EC inputs as the main excitatory inputs for discharge, and other excitatory inputs from hilar mossy cells (Hashimotodani et al., 2017). Therefore, low-pass filtering of SuM inputs could prevent the over-excitation of GCs, leading to anti-seizure effects. In contrast to the presynaptic origin of short-term plasticity at SuM-GC synapses, we previously demonstrated the postsynaptically induced long-term potentiation at SuM-GC synapses, which selectively occurs of glutamatergic co-transmission (Hirai et al., 2022; Tabuchi et al., 2022). Our findings suggest that SuM inputs play diverse roles in modulating GC output via short- and long-term plasticity with pre- and postsynaptic distinct mechanisms, respectively.

Materials and Methods

Animals

C57BL/6 and VGluT2-Cre mice (Jackson Labs, Slc17a6$^{tm2(cre)Lowl}$/J, stock #016963) of either sex aged 6-7 weeks were used for electrophysiological experiments and male C57BL/6 mice at 2–3 months of age were used for anatomical experiments (Figure 4). All animals were group housed in a temperature- and humidity-controlled room under a 12 hr light/12 hr dark cycle. Water and food were provided *ad libitum*. The experiments were approved by the animal care and use committee of Doshisha University and Hokkaido University and were performed in accordance with the guidelines of the committees.

Stereotaxic viral injections

Mice on postnatal days 19 to 21 were placed in a stereotaxic frame, and anesthetized with isoflurane (1.5–2.5%). A beveled glass capillary pipette connected to a microsyringe pump (UMP3, WPI) was used for the viral injection. 200 nL of AAV1-EF1a-DIO-hChR2(H134R)-eYFP (Addgene) was injected into the SuM (relative to bregma, AP: –2.2 mm, ML: ±0.5 mm, DV: –4.85 mm) at a rate of 50 nL/min. The glass capillary was remained at the target site for 5 min before the beginning of the injection and was removed 10 min after infusion.

Hippocampal slice preparation

Acute transverse hippocampal slices (300 μm thick) were prepared from mice 3–4 weeks after AAV injection. The mice were decapitated under isoflurane anesthesia. Briefly, the hippocampi were isolated, embedded in an agar block, and cut using a vibratome (VT1200S, Leica Microsystems) in an ice-cold cutting solution containing (in mM): 215 sucrose, 20 D-glucose, 2.5 KCl, 26 $NaHCO_3$, 1.6 NaH_2PO_4, 1 $CaCl_2$, 4 $MgCl_2$, and 4 $MgSO_4$. Brain blocks, including the interbrain and midbrain, were also isolated and fixed in 4% paraformaldehyde (PFA) for *post hoc* our internal check of the injection site (Tabuchi et al., 2022). Hippocampal slices were transferred to an incubation chamber and incubated at 33.5°C in the cutting solution. After 30 min of incubation, the cutting solution was replaced with an extracellular artificial cerebrospinal fluid (ACSF) containing (in mM): 124 NaCl, 2.5 KCl, 26 $NaHCO_3$, 1 NaH_2PO_4, 2.5 $CaCl_2$, 1.3 $MgSO_4$ and 10 D-glucose at 33.5°C. The slices were stored at room temperature for at least 1 h before recording. Both the cutting solution and the ACSF were oxygenated with 95% O_2 and 5% CO_2. After recovery, slices were transferred to a submersion-type recording chamber for electrophysiological analysis.

Electrophysiology

Whole-cell recordings using an EPC10 (HEKA Electronik) or IPA amplifier (Sutter Instruments) were made from GCs using an infrared differential interference contrast microscopy (IR-DIC, Olympus, BX51WI). We recorded from GCs with an input resistance of < 300 MΩ for mature GCs (Schmidt-Hieber et al., 2004). The data were filtered at 2.9 kHz and sampled at 20 kHz. For voltage-clamp recordings, we used patch pipettes (3–6 MΩ) filled with an intracellular solution with the following composition (in mM): 131 Cs-gluconate, 4 CsCl, 10 HEPES, 0.2 EGTA, 2 Mg-ATP, 0.3 Na_3GTP, 10 phosphocreatine, pH 7.3 adjusted with CsOH (the calculated E_{Cl-} = –90 mV) (292-300 mOsm). For recordings

of synaptic currents at intermediate membrane potentials, 5 mM QX314 was included in the intracellular solution. ChR2-expresing SuM fibers were activated at 0.05 Hz by a pulse of 470 nm blue light (1-5 ms duration, 5.0-10.5 mW/mm^2) delivered through a 40× objective attached to a microscope using an LED (Mightex or ThorLabs). The light intensity was adjusted to yield less than 80% of the maximum response during the baseline period. The illumination field was centered over the recorded cell, unless otherwise stated. Series resistance (8–20 MΩ) was uncompensated and monitored throughout experiments with a –5 mV, 50 ms voltage step, and cells that exhibited a significant change in the series resistance more than 20% were excluded from analysis.

For minimal light stimulation experiments, we first recorded biphasic synaptic responses from GCs by maximum light stimulation of SuM inputs at intermediate membrane potentials from -20 to -30 mV in the presence of 1 μM TTX, 1 mM 4-AP, 50 μM D-AP5, and 1 mM Ca^{2+}. The exact membrane potentials were set to the potential at which the amplitudes of EPSCs and IPSCs were similar. Then, light power intensity was decreased to detect small stochastic synaptic events. We adjusted the light power (<1 ms duration, <1.0 mW/mm^2) to evoke synaptic responses, with a success rate of 15%. A total of 100 trials were recorded every 10 s. EPSC-only responses were determined as the synaptic current with the onset of a downward deflection within 6 ms of light illumination that returned to the baseline without an outward current within 20 ms of light illumination. IPSC-only responses were determined as the synaptic current with the onset of an upward deflection within 6 ms of light illumination, without an inward current immediately after light illumination. Biphasic responses were defined as an EPSC-IPSC sequence, only if an outward peak current following an inward current appeared within 20 ms of light illumination. The amplitude threshold was set to three times the SD of the baseline noise. Based on these criteria, we confirmed that the detection rate of false-positive events (without light illumination) was 0.6 ± 0.4% (3/500 trials, n = 5).

For recordings of asynchronous synaptic events, we initially recorded light stimulation-evoked biphasic synaptic responses at intermediate membrane potentials (-20 to -30 mV) in the presence of Ca^{2+}. The ACSF was then replaced with Ca^{2+}-free ACSF containing 4 mM $SrCl_2$. Asynchronous synaptic responses were evoked by light pulses at 0.1 Hz for 30 times, measured during a 450 ms period beginning 30 ms after the stimulus to exclude the initial synchronous synaptic responses, and analyzed using the Mini Analysis Program (Synaptosoft). D-AP5 (50 μM) was included in the extracellular ACSF throughout the experiment to eliminate NMDA receptor-mediated currents.

For train stimulation, EPSCs were recorded from GCs at a holding potential of -70 mV in the presence of 100 μM picrotoxin, while IPSCs were recorded at a holding potential of 0 mV in the presence of 10 μM NBQX and 50 μM D-AP5. Biphasic PSCs were recorded at a holding potential of -30 mV in the presence of 1 μM TTX, 500 μM 4-AP, and 50 μM D-AP5. In all train-stimulation experiments, 100 μM LY341495 and 3 μM CGP55845 were also added to the ACSF throughout the experiments. 10 light pulses at 5 Hz, 10 Hz, and 20 Hz were delivered every 20 sec, and 10–20 sweeps were recorded.

For field potential recordings in the CA1 region, a recording pipette filled with 1 M NaCl and a patch pipette with broken tip (with diameter of ~20–30 μm) filled with the ACSF were placed in the stratum radiatum of the CA1 region.

For current-clamp recordings, we used an intracellular solution with the following composition (in mM): 135 $KMeSO_4$, 5 KCl, 10 HEPES, 0.2 EGTA, 2 MgATP, 0.3 Na_3GTP, 10 phosphocreatine, pH 7.3 adjusted with NaOH (the calculated E_{Cl-} = –82 mV) (297–299 mOsm). A sinusoidal current was delivered to the soma of GCs at 5 Hz, 10 Hz, and 20 Hz (10 cycles), while the membrane potential was held at -70 mV to -80 mV. The injected current (100–240 pA) was adjusted to generate action potentials with fewer than five spikes in each trial. After obtaining control, a sinusoidal current injection was paired with light stimulation of SuM inputs at the depolarizing phase of each cycle. Subsequently, 100 μM picrotoxin was bath applied, and the same pairing of sinusoidal current with light stimulation were delivered. In each experiment, 10 trials were recorded every 20 sec.

All experiments were performed at 30–33°C in the recording chamber perfused (2 mL/min) with oxygenated ACSF.

Pharmacology

Each reagent was dissolved in water, NaOH or DMSO, depending on the manufacture's recommendation to prepare a stock solution, and stored at –20°C. NBQX, D-AP5, (RS)-baclofen, DCG-IV, γDGG, TPMPA, and LY341495 were purchased from Tocris Bioscience. ω–Conotoxin GVIA and ω–agatoxin IVA were purchased from the Peptide Institute. Picrotoxin was purchased from the Tokyo Chemical Industry. 4-AP and BAPTA-AM were purchased from nacalai tesque. TTX was purchased from Fujifilm Wako Pure Chemical. EGTA-AM was purchased from AAT Bioquest. CGP55845 was purchased from Hello Bio. Reagents were bath applied following dilution into ACSF from the stock solutions immediately before use.

Antibodies

Primary antibodies raised against the following molecules were used: $GABA_A$ receptor γ2 subunit, NMDA receptor GluN1 subunit, VGluT2, VIAAT, and GFP. Information on the molecule, antigen sequence, host species, specificity, reference, NCBI GenBank accession number, and RRID of the primary antibodies used is summarized in Table S1.

Immunohistochemistry for ChR2-expressing SuM terminals

Under deep pentobarbital anesthesia (100 mg/kg of body weight, intraperitoneally), AAV-DIO-ChR2(H134R)-eYFP injected VGluT2-Cre mice were perfused with 4% PFA. Brains were removed and stored in 4% PFA for 4 h at room temperature, then transferred to PBS and left overnight at 4°C. Coronal brain slices containing the SuM or the hippocampus were sectioned at 100 μm using a vibratome (VT1200S, Leica microsystems). After permeabilization in PBS with 1% Triton X-100 for 30 min, the sections were blocked in PBS with 5% donkey serum for 1h. After washing three times with PBS for 10 min each, the sections were incubated in PBS containing primary antibodies and 0.5% Triton X-100 overnight at room temperature. Primary antibodies against GFP (goat, 1:200), VGluT2 (rabbit, 1:200), and VIAAT (guinea pig, 1:200) were used. The sections were then rinsed with PBS three times, and incubated in PBS containing 0.5% Triton X-100 and secondary donkey antibodies (1:500, anti-goat Alexa Fluor 488-conjugated antibody, abcam, ab150129; anti-rabbit Alexa Fluor 568-conjugated antibody, abcam, ab175470; anti-guinea pig Cy5-conjugated antibody, Jackson ImmunoResearch, 706-175-148) for 2h at room temperature. Sections were rinsed three times in PBS and mounted on glass slides with DAPI. To analyze colocalization of ChR2-eYFP-labeled axonal boutons with VGluT2 and VIAAT, z stack images were captured (0.4 μm optical sections) using a fluorescence microscope (BZ-X800, Keyence). Swellings of ChR2-YFP labeled axons were considered as axonal boutons, and their colocalization with VGluT2 and VIAAT immunofluorescence was examined in 3D planes as previously reported (Hashimotodani et al., 2018).

Immunofluorescence using ultrathin sections

Under deep pentobarbital anesthesia (100 mg/kg body weight, i.p.), mice were fixed by transcardially with 5 ml of saline, followed by 60 ml of glyoxal fixative solution (9% glyoxal [Sigma], 8% acetic acid, pH 4.0) (Konno et al., 2023). Brains were dissected and post-fixed at 4°C in glyoxal fixative solution for 2 hr. Coronal 400-μm-thick brain sections were cut on a vibratome (VT1000S, LeicaMicrosystems). Sections were embedded in durcupan (Sigma)

and ultra-thin sections (100 nm-thick) were prepared by Ultracut ultramicrotome (Leica Microsystems). Sections were mounted on silane-coated glass slides (New Silane II, *Muto* Pure Chemicals). After etching with saturated sodium ethanolate solution for 1–5 s, ultra-thin sections on slides were treated with ImmunoSaver (Nisshin EM) at 95°C for 30 min. Sections were blocked with 10% normal donkey serum (Jackson ImmunoResearch) for 20 min, then incubated with a mixture of primary antibody solution (1 μg/ml in phosphate-buffered saline (pH 7.2) containing 0.1% TritonX-100 (PBST) overnight at room temperature. Sections were washed three times with PBST and incubated with a solution of Alexa488, Cy3, and Alexa647-labeled species-specific secondary antibodies (Jackson ImmunoResearch; Thermo Fisher Scientific) diluted at 1:200 in PBST for 2 h at room temperature. After washing, sections were air-dried, and mounted with using ProLong Glass (Thermo Fisher Scientific). Photographs were taken with a confocal laser microscope (FV1200, Evident) using 20x and 60x objectives.

Postembedding immunoelectron microscopy

Under deep anesthesia with pentobarbital (100 mg/kg, i.p.), mice were transcardially perfused with 4% PFA/0.1 M PB (pH 7.2) for 10 min, brains were removed, postfixed for 2 h in the same fixative, and coronal sections (400 μm-thick) prepared using a vibratome (VT1000S, Leica Microsystems). Then, sections were cryoprotected with 30% glycerol in PB, and frozen rapidly with liquid propane in the EM CPC unit (Leica Microsystems). Frozen sections were immersed in 0.5% uranyl acetate in methanol at –90°C in the AFS freeze-substitution unit (Leica Microsystems), infiltrated at –45°C with Lowicryl HM-20 resin (Chemische Werke Lowi, Waldkraiburg, Germany), and polymerized with ultraviolet light. Ultrathin sections were made using an Ultracut ultramicrotome (Leica Microsystems). Ultrathin sections (100 nm thick) mounted on nickel grids were etched with ultrathin sections on nickel grids were etched with saturated sodium-ethanolate solution for 1–5 s. For double labeling against VGluT2 and VIAAT, sections were incubated in blocking solution containing 2% normal goat serum (Nichirei, Tokyo, Japan) in 0.03% Triton X-100 in Tris-buffered saline (TBST, pH 7.4), followed by VIAAT antibody (20 μg/ml) diluted in 2% normal goat serum in TBST overnight, then colloidal gold-conjugated (5 nm) anti-rabbit IgG in blocking solution for 2 hr. After extensive washing in distilled water, sections were incubated in blocking solution containing 2% rabbit serum (Nichirei, Tokyo, Japan) in TBST for 10 min, VGluT2 antibody (20 μg/ml) diluted with 2% normal rabbit serum in TBST overnight, and colloidal gold-conjugated (10 nm) anti-guinea pig IgG in blocking solution for 2 hr. After extensive

washing in distilled water, sections were fixed with 2% OsO4 for 15 min, then stained with 5% uranyl acetate/40% EtOH for 90 s and Reynold's lead citrate solution for 60 s. Photographs were taken from the granular layer of the dentate gyrus with an H-7100 electron microscope at x20,000 magnification.

Data analysis

The PPR was defined as the ratio of the amplitude of the second PSCs to the amplitude of the first PSCs (100 ms inter-stimulus interval). The reduction in PSCs by a decrease in extracellular Ca^{2+} concentration was determined by comparing 10 min baseline responses (2.5 mM Ca^{2+}) with responses 20–25 min after replacement of extracellular Ca^{2+} (1 mM). The inhibition of PSCs by DCG-IV, baclofen, ω-CgTx, ω–Aga-IVA, BAPTA-AM, and EGTA-AM was determined by comparing the 10 min baseline responses with responses at 15–20 min (or 25–30 min for BAPTA-AM, and EGTA-AM) after each drug application. The PSCs probability was calculated as the percentage of the number of synaptic responses among 100 sweeps. Train stimulation-induced depression was calculated as the ratio of the amplitude of the second to 10th PSCs to the amplitude of the first PSCs. Each stimulus point had an averaged of 10–20 sweeps. Spike probability was calculated as the percentage of the number of spikes among 10 trials.

Statistics

Statistical analyses were performed using OriginPro software (OriginLab, USA). Normality of the distributions was assessed using the Shapiro–Wilk test. For samples with normal distributions, Student's unpaired and paired two-tailed t tests were used to assess the between-group and within-group differences, respectively. For samples that were not normally distributed, a non-parametric paired sample Wilcoxon signed-rank test was used. The Kolmogorov–Smirnov test was used for cumulative distributions. Differences among two or multiple samples were assessed by using one-way or two-way ANOVA followed by Tukey's *post hoc* test for multiple comparisons. Statistical significance was set at $p < 0.05$ (***, **, and * indicates $p < 0.001$, $p < 0.01$ and $p < 0.05$, respectively). All values are reported as the mean ± SEM.

Acknowledgement

This work was supported by the Grants-in-Aid for Scientific Research (24KJ2139 to H. H.; 20KK0171 and 24K02125 to T.S.; 20H03358, 23H04240, and 23K18167 to Y.H.) from Japan Society for the Promotion of Science (JSPS), the Takeda Science Foundation (to Y.H.), the Naito Foundation (to Y.H.), the Mochida Memorial Foundation for Medical and Pharmaceutical Research (to Y.H.) and JSPS Core-to-Core Program A. Advanced Research Networks (grant number: JPJSCCA20220007 to T.S.).

Author contributions

T.S. and Y.H. designed the experiments. H.H. and Y.H. performed the experiments and data analysis. K.K., M.Y. and M.W. designed and performed the immunohistochemistry experiments. Y.H. wrote the manuscript with input from all authors.

Declaration of interests

The authors declare no competing interests.

References

Adler EM, Augustine GJ, Duffy SN, Charlton MP (1991) Alien intracellular calcium chelators attenuate neurotransmitter release at the squid giant synapse. J Neurosci 11:1496-1507.

Ajibola MI, Wu JW, Abdulmajeed WI, Lien CC (2021) Hypothalamic Glutamate/GABA Cotransmission Modulates Hippocampal Circuits and Supports Long-Term Potentiation. J Neurosci 41:8181-8196.

Billwiller F, Castillo L, Elseedy H, Ivanov AI, Scapula J, Ghestem A, Carponcy J, Libourel PA, Bras H, Abdelmeguid NE, Krook-Magnuson E, Soltesz I, Bernard C, Luppi PH, Esclapez M (2020) GABA-glutamate supramammillary neurons control theta and gamma oscillations in the dentate gyrus during paradoxical (REM) sleep. Brain Struct Funct 225:2643-2668.

Boulland JL, Jenstad M, Boekel AJ, Wouterlood FG, Edwards RH, Storm-Mathisen J, Chaudhry FA (2009) Vesicular glutamate and GABA transporters sort to distinct sets of vesicles in a population of presynaptic terminals. Cereb Cortex 19:241-248.

Brenowitz S, Trussell LO (2001) Minimizing synaptic depression by control of release probability. J Neurosci 21:1857-1867.

Chen S, He L, Huang AJY, Boehringer R, Robert V, Wintzer ME, Polygalov D, Weitemier AZ, Tao Y, Gu M, Middleton SJ, Namiki K, Hama H, Therreau L, Chevaleyre V, Hioki H, Miyawaki A, Piskorowski RA, McHugh TJ (2020) A hypothalamic novelty signal modulates hippocampal memory. Nature 586:270-274.

Eccles JC, Fatt P, Koketsu K (1954) Cholinergic and inhibitory synapses in a pathway from motor-axon collaterals to motoneurones. J Physiol 126:524-562.

Eggermann E, Bucurenciu I, Goswami SP, Jonas P (2011) Nanodomain coupling between Ca(2)(+) channels and sensors of exocytosis at fast mammalian synapses. Nat Rev Neurosci 13:7-21.

Farrell JS, Lovett-Barron M, Klein PM, Sparks FT, Gschwind T, Ortiz AL, Ahanonu B, Bradbury S, Terada S, Oijala M, Hwaun E, Dudok B, Szabo G, Schnitzer MJ, Deisseroth K, Losonczy A, Soltesz I (2021) Supramammillary regulation of locomotion and hippocampal activity. Science 374:1492-1496.

Farsi Z, Preobraschenski J, van den Bogaart G, Riedel D, Jahn R, Woehler A (2016) Single-vesicle imaging reveals different transport mechanisms between glutamatergic and GABAergic vesicles. Science 351:981-984.

Foster KA, Regehr WG (2004) Variance-mean analysis in the presence of a rapid antagonist indicates vesicle depletion underlies depression at the climbing fiber synapse. Neuron 43:119-131.

Hashimotodani Y, Karube F, Yanagawa Y, Fujiyama F, Kano M (2018) Supramammillary Nucleus Afferents to the Dentate Gyrus Co-release Glutamate and GABA and Potentiate Granule Cell Output. Cell Rep 25:2704-2715 e2704.

Hashimotodani Y, Nasrallah K, Jensen KR, Chavez AE, Carrera D, Castillo PE (2017) LTP at Hilar Mossy Cell-Dentate Granule Cell Synapses Modulates Dentate Gyrus Output by Increasing Excitation/Inhibition Balance. Neuron 95:928-943 e923.

Heine M, Groc L, Frischknecht R, Beique JC, Lounis B, Rumbaugh G, Huganir RL, Cognet L, Choquet D (2008) Surface mobility of postsynaptic AMPARs tunes synaptic transmission. Science 320:201-205.

Hirai H, Sakaba T, Hashimotodani Y (2022) Subcortical glutamatergic inputs exhibit a Hebbian form of long-term potentiation in the dentate gyrus. Cell Rep 41:111871.

Hnasko TS, Edwards RH (2012) Neurotransmitter corelease: mechanism and physiological role. Annu Rev Physiol 74:225-243.

Ito HT, Moser EI, Moser MB (2018) Supramammillary Nucleus Modulates Spike-Time Coordination in the Prefrontal-Thalamo-Hippocampal Circuit during Navigation. Neuron 99:576-587 e575.

Jackman SL, Beneduce BM, Drew IR, Regehr WG (2014) Achieving high-frequency optical control of synaptic transmission. J Neurosci 34:7704-7714.

Kamondi A, Acsady L, Wang XJ, Buzsaki G (1998) Theta oscillations in somata and dendrites of hippocampal pyramidal cells in vivo: activity-dependent phase-precession of action potentials. Hippocampus 8:244-261.

Kesner AJ, Mozaffarilegha M, Thirtamara Rajamani K, Arima Y, Harony-Nicolas H, Hashimotodani Y, Ito HT, Song J, Ikemoto S (2023) Hypothalamic Supramammillary Control of Cognition and Motivation. J Neurosci 43:7538-7546.

Kim S, Sabatini BL (2023) Analytical approaches to examine gamma-aminobutyric acid and glutamate vesicular co-packaging. Frontiers in Synaptic Neuroscience 14.

Kim S, Wallace ML, El-Rifai M, Knudsen AR, Sabatini BL (2022) Co-packaging of opposing neurotransmitters in individual synaptic vesicles in the central nervous system. Neuron 110:1371-1384 e1377.

Kirk IJ, McNaughton N (1991) Supramammillary cell firing and hippocampal rhythmical slow activity. Neuroreport 2:723-725.

Kocsis B, Vertes RP (1994) Characterization of neurons of the supramammillary nucleus and mammillary body that discharge rhythmically with the hippocampal theta rhythm in the rat. J Neurosci 14:7040-7052.

Konno K, Yamasaki M, Miyazaki T, Watanabe M (2023) Glyoxal fixation: An approach to solve immunohistochemical problem in neuroscience research. Sci Adv 9:eadf7084.

Lee S, Kim K, Zhou ZJ (2010) Role of ACh-GABA cotransmission in detecting image motion and motion direction. Neuron 68:1159-1172.

Li Y, Bao H, Luo Y, Yoan C, Sullivan HA, Quintanilla L, Wickersham I, Lazarus M, Shih YI, Song J (2020) Supramammillary nucleus synchronizes with dentate gyrus to regulate spatial memory retrieval through glutamate release. Elife 9.

Ma S, Hangya B, Leonard CS, Wisden W, Gundlach AL (2018) Dual-transmitter systems regulating arousal, attention, learning and memory. Neurosci Biobehav Rev 85:21-33.

Magee JC (2001) Dendritic mechanisms of phase precession in hippocampal CA1 pyramidal neurons. J Neurophysiol 86:528-532.

Markwardt SJ, Wadiche JI, Overstreet-Wadiche LS (2009) Input-specific GABAergic signaling to newborn neurons in adult dentate gyrus. J Neurosci 29:15063-15072.

Neher E, Brose N (2018) Dynamically Primed Synaptic Vesicle States: Key to Understand Synaptic Short-Term Plasticity. Neuron 100:1283-1291.

Nusbaum MP, Blitz DM, Swensen AM, Wood D, Marder E (2001) The roles of co-transmission in neural network modulation. Trends Neurosci 24:146-154.

Pedersen NP, Ferrari L, Venner A, Wang JL, Abbott SBG, Vujovic N, Arrigoni E, Saper CB, Fuller PM (2017) Supramammillary glutamate neurons are a key node of the arousal system. Nat Commun 8:1405.

Robert V, Therreau L, Chevaleyre V, Lepicard E, Viollet C, Cognet J, Huang AJ, Boehringer R, Polygalov D, McHugh TJ, Piskorowski RA (2021) Local circuit allowing hypothalamic control of hippocampal area CA2 activity and consequences for CA1. Elife 10.

Root DH, Mejias-Aponte CA, Zhang S, Wang HL, Hoffman AF, Lupica CR, Morales M (2014) Single rodent mesohabenular axons release glutamate and GABA. Nat Neurosci 17:1543-1551.

Root DH, Zhang S, Barker DJ, Miranda-Barrientos J, Liu B, Wang HL, Morales M (2018) Selective Brain Distribution and Distinctive Synaptic Architecture of Dual Glutamatergic-GABAergic Neurons. Cell Rep 23:3465-3479.

Rost BR, Wietek J, Yizhar O, Schmitz D (2022) Optogenetics at the presynapse. Nat Neurosci 25:984-998.

Sakaba T (2008) Two Ca(2+)-dependent steps controlling synaptic vesicle fusion and replenishment at the cerebellar basket cell terminal. Neuron 57:406-419.

Schmidt-Hieber C, Jonas P, Bischofberger J (2004) Enhanced synaptic plasticity in newly generated granule cells of the adult hippocampus. Nature 429:184-187.

Shabel SJ, Proulx CD, Piriz J, Malinow R (2014) Mood regulation. GABA/glutamate co-release controls habenula output and is modified by antidepressant treatment. Science 345:1494-1498.

Silm K, Yang J, Marcott PF, Asensio CS, Eriksen J, Guthrie DA, Newman AH, Ford CP, Edwards RH (2019) Synaptic Vesicle Recycling Pathway Determines Neurotransmitter Content and Release Properties. Neuron 102:786-800 e785.

Soussi R, Zhang N, Tahtakran S, Houser CR, Esclapez M (2010) Heterogeneity of the supramammillary-hippocampal pathways: evidence for a unique GABAergic neurotransmitter phenotype and regional differences. Eur J Neurosci 32:771-785.

Sudhof TC (2013) Neurotransmitter release: the last millisecond in the life of a synaptic vesicle. Neuron 80:675-690.

Tabuchi E, Sakaba T, Hashimotodani Y (2022) Excitatory selective LTP of supramammillary glutamatergic/GABAergic cotransmission potentiates dentate granule cell firing. Proc Natl Acad Sci U S A 119:e2119636119.

Takacs VT, Cserep C, Schlingloff D, Posfai B, Szonyi A, Sos KE, Kornyei Z, Denes A, Gulyas AI, Freund TF, Nyiri G (2018) Co-transmission of acetylcholine and GABA regulates hippocampal states. Nat Commun 9:2848.

Tritsch NX, Granger AJ, Sabatini BL (2016) Mechanisms and functions of GABA co-release. Nat Rev Neurosci 17:139-145.

Trudeau LE, El Mestikawy S (2018) Glutamate Cotransmission in Cholinergic, GABAergic and Monoamine Systems: Contrasts and Commonalities. Front Neural Circuits 12:113.

Trudeau LE, Hnasko TS, Wallen-Mackenzie A, Morales M, Rayport S, Sulzer D (2014) The multilingual nature of dopamine neurons. Prog Brain Res 211:141-164.

Trussell LO, Zhang S, Raman IM (1993) Desensitization of AMPA receptors upon multiquantal neurotransmitter release. Neuron 10:1185-1196.

Turecek J, Jackman SL, Regehr WG (2016) Synaptic Specializations Support Frequency-Independent Purkinje Cell Output from the Cerebellar Cortex. Cell Rep 17:3256-3268.

Uchigashima M, Yamazaki M, Yamasaki M, Tanimura A, Sakimura K, Kano M, Watanabe M (2011) Molecular and morphological configuration for 2-arachidonoylglycerol-mediated retrograde signaling at mossy cell-granule cell synapses in the dentate gyrus. J Neurosci 31:7700-7714.

Vaaga CE, Borisovska M, Westbrook GL (2014) Dual-transmitter neurons: functional implications of co-release and co-transmission. Curr Opin Neurobiol 29:25-32.

Wadiche JI, Jahr CE (2001) Multivesicular release at climbing fiber-Purkinje cell synapses. Neuron 32:301-313.

Wallace ML, Sabatini BL (2023) Synaptic and circuit functions of multitransmitter neurons in the mammalian brain. Neuron 111:2969-2983.

Wallace ML, Saunders A, Huang KW, Philson AC, Goldman M, Macosko EZ, McCarroll SA, Sabatini BL (2017) Genetically Distinct Parallel Pathways in the Entopeduncular Nucleus for Limbic and Sensorimotor Output of the Basal Ganglia. Neuron 94:138-152 e135.

Wong AY, Graham BP, Billups B, Forsythe ID (2003) Distinguishing between presynaptic and postsynaptic mechanisms of short-term depression during action potential trains. J Neurosci 23:4868-4877.

Wu LG, Saggau P (1994) Pharmacological identification of two types of presynaptic voltage-dependent calcium channels at CA3-CA1 synapses of the hippocampus. J Neurosci 14:5613-5622.

Yoo JH, Zell V, Gutierrez-Reed N, Wu J, Ressler R, Shenasa MA, Johnson AB, Fife KH, Faget L, Hnasko TS (2016) Ventral tegmental area glutamate neurons co-release GABA and promote positive reinforcement. Nat Commun 7:13697.

Zucker RS, Regehr WG (2002) Short-term synaptic plasticity. Annu Rev Physiol 64:355-405.

Zych SM, Ford CP (2022) Divergent properties and independent regulation of striatal dopamine and GABA co-transmission. Cell Rep 39:110823.

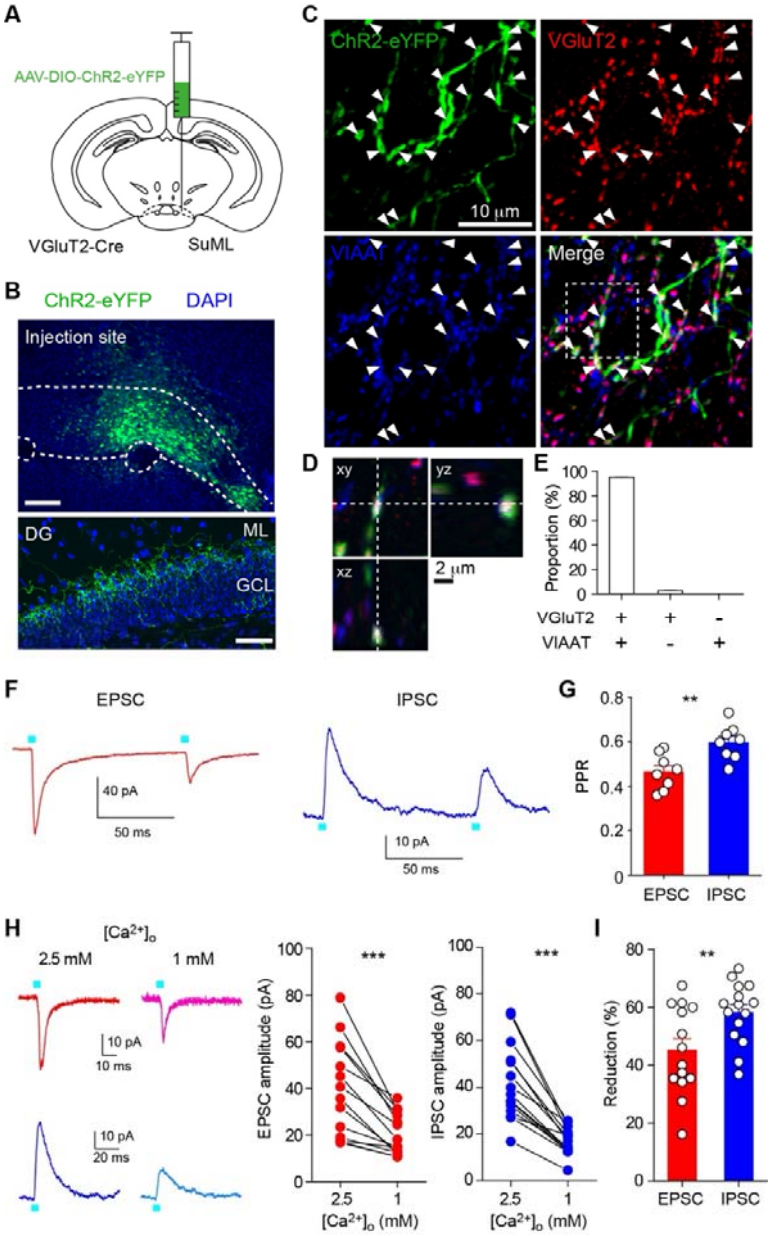

Figure 1. Different PPRs and Ca^{2+} sensitivities of glutamate/GABA co-transmission at SuM-GC synapses

(**A**) Diagram illustrating the injection of AAV-DIO-ChR2(H134R)-eYFP into the lateral part of SuM of VGluT2-Cre mouse. (**B**) (top) Fluorescence image showing the injection site of AAV in the SuM. (bottom) ChR2(H134R)-eYFP-expressing SuM axons are observed in the supragranular layer of the DG. ML, molecular layer; GCL, granule cell layer. Scale bars, Top, 200 μm; Bottom, 50 μm. (**C**) Z-stacked immunofluorescence images double stained for VGluT2 (red) and VIAAT (blue). The merged image demonstrates the colocalization of VGluT2 and VIAAT in the ChR2-eYFP-expressing SuM terminals (arrowheads). (**D**) Higher

magnification xy, xz, and yz projection images outlined in boxed area in (C) show that a SuM bouton is co-stained with VGluT2 and VIAAT. (**E**) Proportion of VGluT2- and/or VIAAT-expressing boutons in the ChR2-eYFP labeled boutons (2205 boutons, 7 slices). Both VGluT2 and VIAAT (95.2 ± 0.3%), VGluT2 only (2.7 ± 0.2%), and VIAAT only (0%). (**F**) Representative traces of EPSC (red, V_h = -70 mV) and IPSC (blue, V_h = 0 mV) evoked with paired pulse illumination (100 ms interval). (**G**) Summary plot of PPR showing a significant difference between EPSC and IPSC. (**H**) Representative traces (left) and summary plots (right) of EPSCs and IPSCs in 2.5 and 1 mM extracellular Ca^{2+}. (**I**) Summary plot of percent reduction in the amplitudes of EPSCs and IPSCs from 2.5 to 1 mM extracellular Ca^{2+}. Data are presented as mean ± SEM. **$p < 0.01$, ***$p < 0.001$.

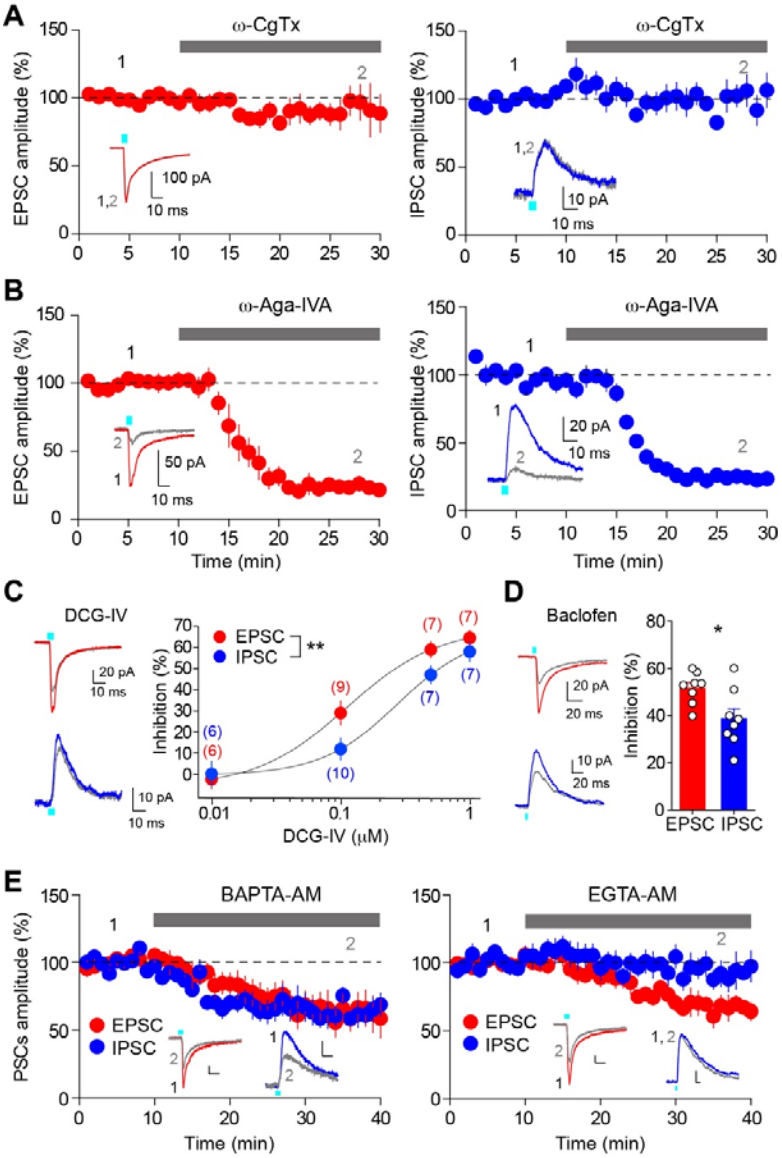

Figure 2. Different presynaptic modulation and Ca^{2+} chelator-sensitivities of glutamate/GABA co-transmission

(**A**) Time course summary plots showing the effects of ω-CgTx (500 nM) on co-transmission of glutamate (left) and GABA (right) at SuM-GC synapses. Insets indicate representative traces. (**B**) Time course summary plots showing that the co-transmission of glutamate (left) and GABA (right) at SuM-GC synapses were inhibited by ω-Aga-IVA (200 nM). Insets show representative traces. (**C**) (left) Representative traces before (EPSC, red; IPSC, blue) and after (gray) application of DCG-IV (0.1 μM). (right) Summary plot of concentration-response curves. Data are fitted to the Hill equation. Numbers in parentheses indicate the number of

cells. (**D**) (left) Representative traces before (EPSC, red; IPSC, blue) and after (gray) application of baclofen (5 μM). (right) Summary plot of percent inhibition in the amplitudes of EPSCs and IPSCs by 5 μM baclofen. (**E**) Time course summary plots showing the sensitivity of EPSCs and IPSCs to 100 μM BAPTA-AM (left) and 100 μM EGTA-AM (right). Insets show representative traces. Calibration: 10 pA, 10 ms. Data are presented as mean ± SEM. *$p < 0.05$, **$p < 0.01$.

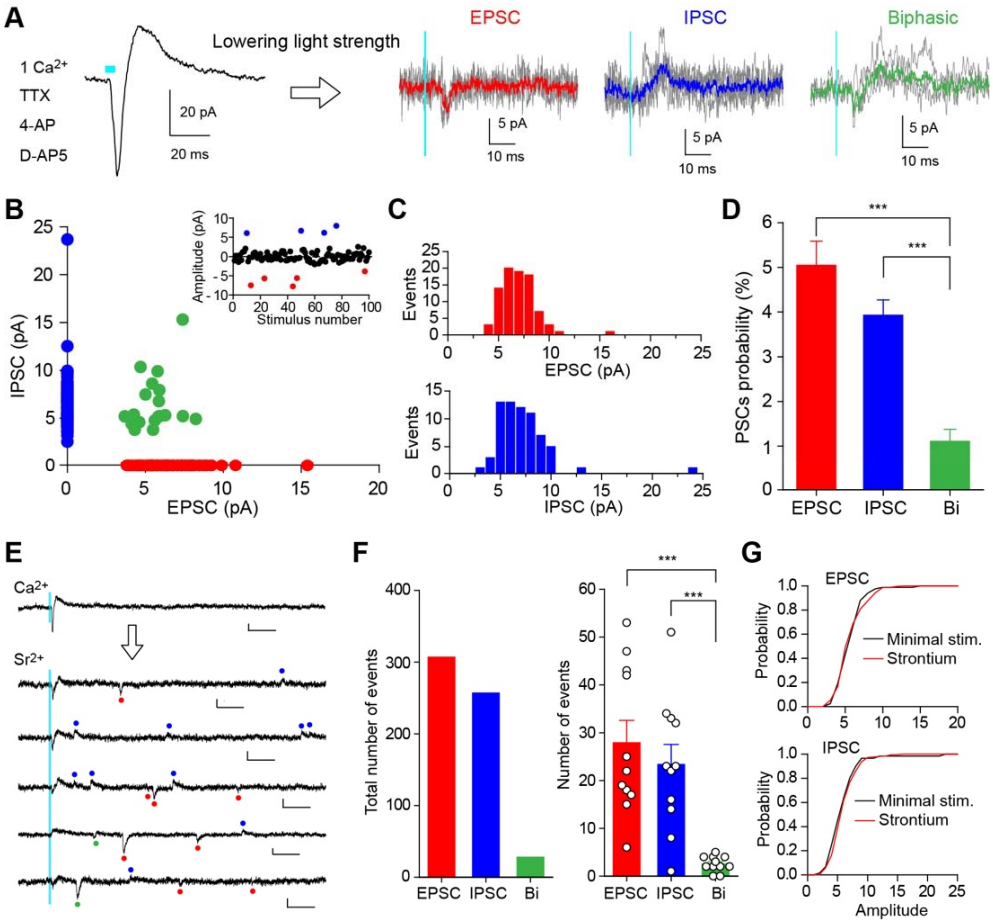

Figure 3. Uniquantal release-mediated synaptic responses evoked by minimal light stimulation or strontium-induced asynchronous release at SuM-GC synapses

(**A**) Representative traces of biphasic response elicited by light stimulation with maximum light power (left) and stochastically evoked PSCs with minimal light stimulation (100 trials for each cell) (right). Synaptic responses at SuM-GC synapses were recorded at holding potentials of -20 to -30 mV in the presence of TTX (1 μM), 4-AP (1 mM), D-AP5 (50 μM), and Ca^{2+} (1 mM). Average EPSC (red), IPSC (blue), and biphasic current (green) are superimposed on individual traces. (**B**) Scatter plot of the amplitude of IPSCs against the amplitude of EPSCs recorded from 17 cells. Success events of 172 PSCs are plotted. (Inset) A single experiment showing 100 trials with an interval of 10 sec elicited stochastically EPSCs (red) and IPSCs (blue). (**C**) Amplitude histograms of EPSCs (top) and IPSCs (bottom) in same data as in B. (**D**) Summary graph of PSCs probability. (**E**) Representative traces showing strontium-induced asynchronous release recorded from GC at holding potentials of -20 to -30 mV. The NMDA receptor antagonist D-AP5 (50 μM) was included in the extracellular solution to eliminate NMDA receptor-mediated EPSCs. Red, blue, and green

points indicate detected EPSCs, IPSCs, and biphasic currents, respectively. Calibration: 10 pA, 50 ms. (**F**) (left) Summary bar graph showing the total number of asynchronous quantal responses (n = 11, 30 trials for each cell) (EPSC: 307 events; IPSC: 257 events; biphasic: 28 events). (right) Averaged number of asynchronous events showing that the majority of asynchronous events are EPSCs and IPSCs, and a few biphasic responses. (**G**) Cumulative distributions of the amplitudes of EPSCs (top) and IPSCs (bottom) for minimal light stimulation-evoked PSCs and strontium-induced PSCs (EPSC: minimal stim.: 86 events from 17 cells; strontium: 307 events from 11 cells, $p = 0.72$; IPSC: minimal stim.: 67 events from 17 cells; strontium: 256 events from 11 cells, $p = 0.096$, Kolmogorov-Smirnov test). Data are presented as mean ± SEM. ***$p < 0.001$.

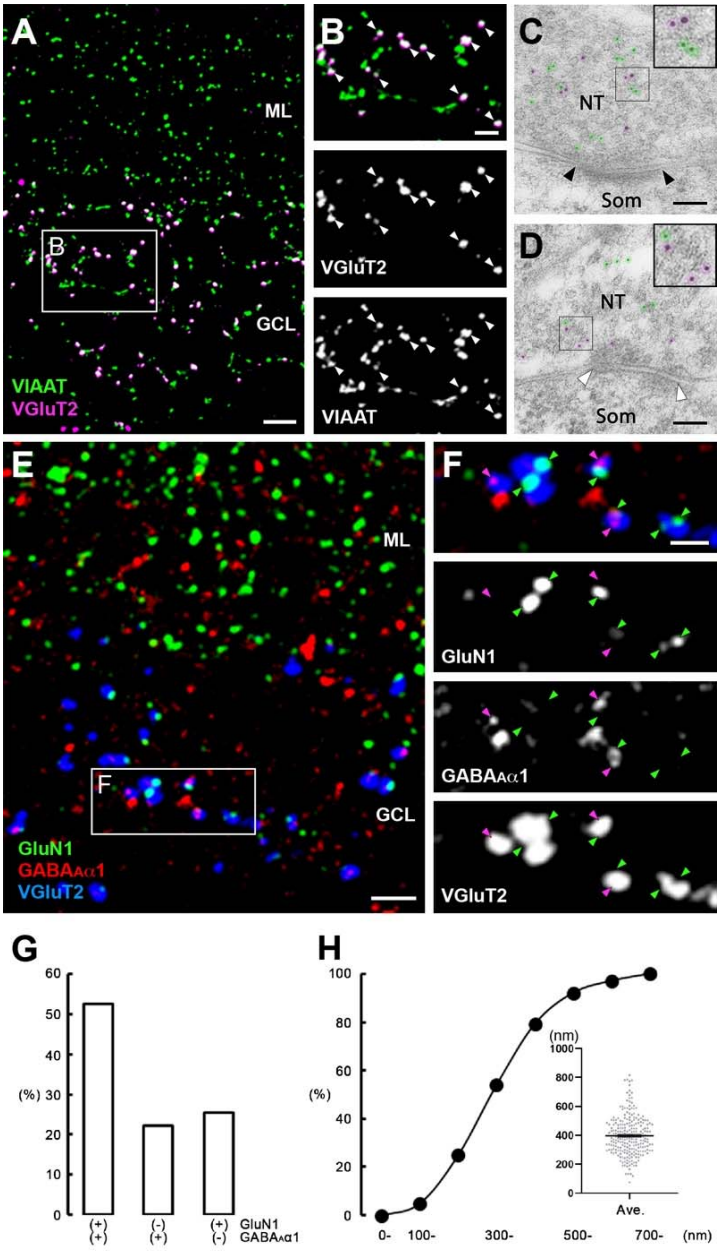

Figure 4. Close association of GluN1 and GABA$_A$α1 facing the same SuM terminals

(**A, B**) Double immunofluorescence for VIAAT (green) and VGluT2 (magenta) in the GC layer of the DG. (B) Higher magnification images of the boxed area in (A) show VGluT2-positive terminals are co-labeled with VIAAT (white arrowheads). (**C, D**) Post-embedding immunogold electron microscopy showing that immunogold particles for VIAAT (magenta, 5 nm) and VGluT2 (green, 10 nm) and are co-exist in the same SuM terminals of asymmetric (C) and symmetric (D) synapses. NT, nerve terminal; Som, soma. (**E, F**) Triple immunofluorescence for GluN1 (green), GABA$_A$α1 (red), and VGluT2 (blue) in the

GC layer of the DG. (F) Higher magnification images of the boxed region in E. Green and magenta arrowheads indicate GluN1 or $GABA_A\alpha1$ puncta that are apposed to VGluT2 puncta, respectively. (**G**) Proportion of GluN1 and $GABA_A\alpha1$ puncta in close proximity to 634 VGluT2-positive SuM terminals. (**H**) Cumulative distribution of the distance between GluN1 and $GABA_A\alpha1$ puncta derived from 241 VGluT2-positive SuM terminals that are double-labeled for GluN1 and $GABA_A\alpha1$. Individual and average values are plotted in inset. Data were obtained from two mice. Scale bars: A, 5 μm; B, E, 2 μm; C, D, 100 nm; F, 1 μm.

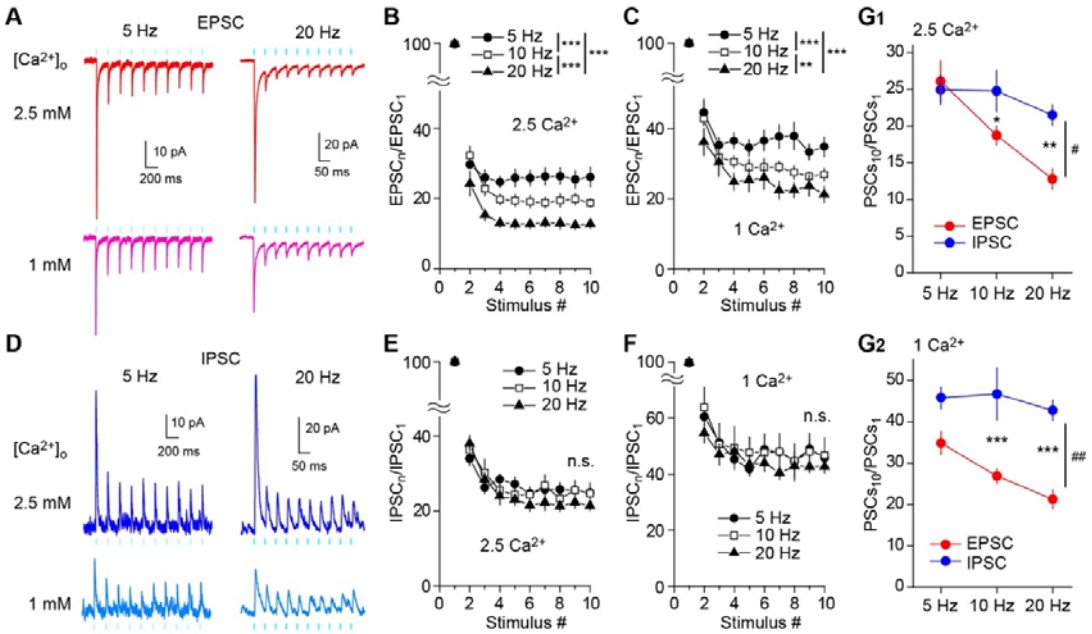

Figure 5. Frequency-dependent shift of glutamate/GABA co-transmission balance of SuM inputs in GCs

(**A, D**) Representative traces of EPSCs (V_h = -70 mV) (A) and IPSCs (V_h = 0 mV) (D) in response to 10 light stimuli at 5 Hz (left) or 20 Hz (right) in 2.5 mM (top) or 1 mM (bottom) extracellular Ca^{2+}. (**B**) Summary graph of normalized EPSC amplitude plotted against the stimulus number in 2.5 mM extracellular Ca^{2+}. Two-way repeated measures ANOVA, $F_{(2,16)}$ = 13.0, $p < 0.001$, n = 9 or 10; Tukey post hoc test: ***$p < 0.001$. (**C**) Same as (B), but recorded in 1 mM extracellular Ca^{2+}. Two-way repeated measures ANOVA, $F_{(2,16)}$ = 11.4, $p < 0.001$, n = 9 or 10; Tukey post hoc test: **$p < 0.01$, ***$p < 0.001$. (**E**) Summary graph of normalized IPSC amplitude plotted against stimulus number in 2.5 mM extracellular Ca^{2+}. Two-way repeated measures ANOVA, $F_{(2,16)}$ = 0.003, p = 0.997, n = 9. (**F**) Same as (E), but recorded in 1 mM extracellular Ca^{2+}. Two-way repeated measures ANOVA, $F_{(2,16)}$ = 0.02, p = 0.981, n = 9. (**G**) Summary plots showing the normalized amplitudes of 10th EPSCs and IPSCs at 5 Hz, 10 Hz, and 20 Hz in 2.5 mM extracellular Ca^{2+} (G1: two-way repeated measures ANOVA, $F_{(1,7)}$ = 8.03, $^{\#}p < 0.05$, n = 9 or 10; Tukey's post hoc test, EPSC versus IPSC, *$p < 0.05$, **$p < 0.01$), or in 1 mM extracellular Ca^{2+} (G2: two-way repeated measures ANOVA, $F_{(1,7)}$ = 21.76, $^{\#\#}p < 0.01$, n = 9 or 10; Tukey's post hoc test, EPSC versus IPSC, ***$p < 0.001$). n.s., not significant. Data are presented as mean ± SEM.

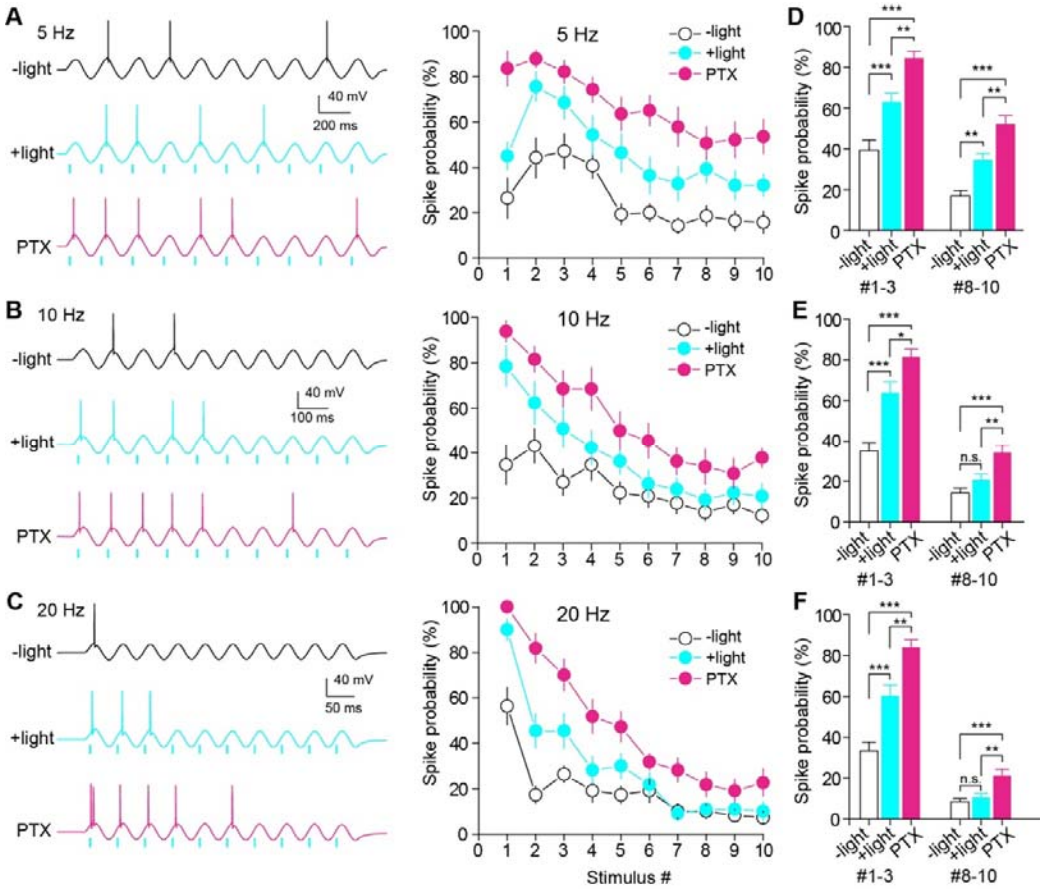

Figure 6. Frequency-dependent modulation of GC firing by SuM inputs

(**A-C**) (left) Representative traces showing GC spikes in response to sinusoidal current injections without (top) and with (middle) paired light stimulation of SuM inputs at 5 Hz (A), 10 Hz (B), and 20 Hz (C). Bottom trace showing the GC response to sinusoidal current injection paired with light stimulation in the presence of 100 μM picrotoxin (PTX). (right) Summary graph of spike probability against stimulus number. (**D-F**) Summary plots of spike probability at initial and last three stimulus numbers at 5 Hz (D), 10 Hz (E), and 20 Hz (F). The spike probabilities of stimulus numbers 1-3 and 8-10 were averaged. (D) one-way ANOVA, n = 14, $F_{(2,123)} = 28.8$, $p < 0.001$ (#1-3), $F_{(2,123)} = 25.8$, $p < 0.001$ (#8-10); Tukey's post hoc test, ***p < 0. 001, **p < 0. 01. (E) one-way ANOVA, n = 13, $F_{(2,114)} = 26.3$, $p < 0.001$ (#1-3), $F_{(2,114)} = 11.8$, $p < 0.001$ (#8-10); Tukey's post hoc test, ***p < 0. 001, **p < 0. 01, *p < 0.05, n.s., not significant. (F) one-way ANOVA, n = 11, $F_{(2,96)} = 31.4$, $p < 0.001$ (#1-3), $F_{(2,96)} = 9.2$, $p < 0.001$ (#8-10); Tukey's post hoc test, ***p < 0. 001, **p < 0.01, n.s., not significant. Data are presented as mean ± SEM.

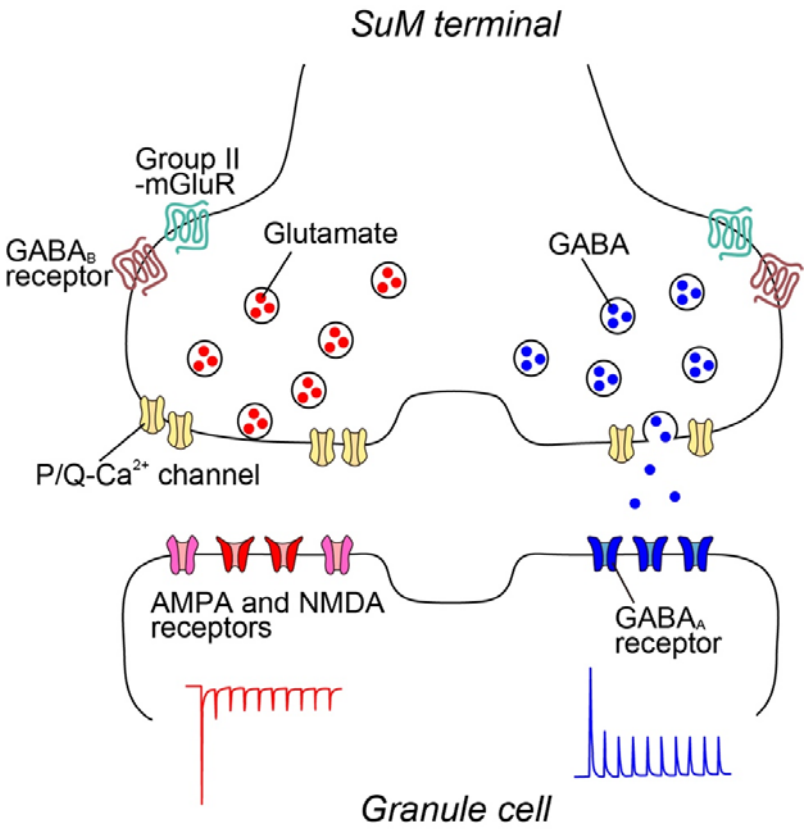

Figure 7. Working hypothesis of synaptic architecture of SuM-GC synapse

A single SuM terminal contains distinct glutamatergic and GABAergic vesicles, which are regulated by P/Q-type Ca^{2+} channels and also modulated by group II mGluRs and $GABA_B$ receptors. Glutamatergic and GABAergic vesicles are loosely and tightly coupled with Ca^{2+} channels, respectively. At the postsynaptic site of GCs, AMPA/NMDA and $GABA_A$ receptors are distributed separately. Based on their molecular composition, glutamatergic and GABAergic synapses are established independently, achieving the distinct glutamatergic and GABAergic transmission.

Supplementary Figures

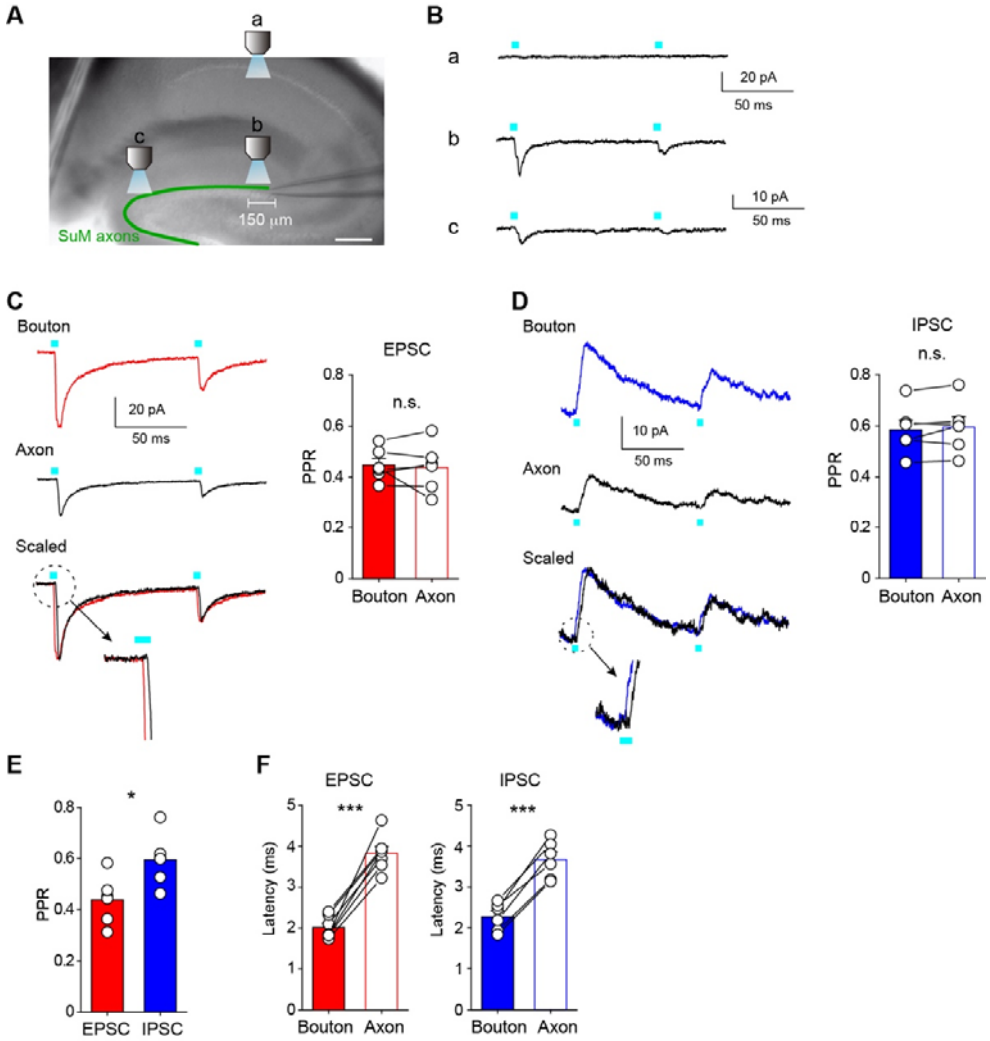

Figure S1. PPRs of glutamatergic and GABAergic co-transmission show no difference between over-axon and over-bouton illumination (Related to Figure 1)

(A) Diagram of the experimental setup. We recorded from GCs located in the most edge of upper blade of GC layer (~150 μm). Once synaptic responses were observed by over-bouton illumination (over-the recorded cell soma, position b), then the objective lens was moved to ~600 μm vertically away in the stratum radiatum of the CA1 region (position a). The light power was adjusted to evoke no response at position a, indicating that SuM-GC synapses on the recorded GCs were out of the illumination field. The objective lens was then returned to position b, and PSCs of SuM-GC synapses were recorded with paired stimulation. Then, the objective lens was moved ~600 μm along the GC layer (position c) to achieve over-axon illumination. Scale bar: 200 μm. **(B)** Representative traces of SuM-GC EPSCs evoked with

over-CA1 (a), over-bouton (b), and over-axon (c) illumination. **(C, D)** Representative traces (left) and summary plots of PPRs (right) of SuM-GC EPSCs (C) or IPSCs (D) indicating no significant difference between over-bouton and over-axon illumination of SuM inputs (EPSC: bouton: 0.45 ± 0.03; axon: 0.44 ± 0.04, $n = 6$, $p = 0.72$, paired t-test; IPSC: bouton: 0.58 ± 0.04; axon: 0.59 ± 0.04, $n = 6$, $p = 0.32$, paired t-test). EPSCs or IPSCs were recorded with over-bouton (top) or over-axon (middle) illumination, respectively. Bottom traces show that a trace by over-axon stimulation was scaled to the peak of a trace by over-bouton stimulation. Magnified traces of the dotted circle show a delayed onset latency of a trace by over-axon stimulation relative to a trace by over-bouton stimulation. **(E)** Summary plot of PPR indicating a significant difference between EPSC and IPSC evoked by over-axon illumination (EPSC: 0.44 ± 0.04; IPSC: 0.59 ± 0.04, $n = 6$, $p < 0.05$, unpaired t-test). **(F)** Summary plots of latency to the onset of the synaptic response. The delayed latency of the synaptic responses by over-axon illumination indicates that synaptic transmission was mediated by light-evoked action potential propagation toward SuM terminals (EPSC: bouton: 2.0 ± 0.1 ms; axon: 3.8 ± 0.2 ms, $n = 7$, $p < 0.001$, paired t-test; IPSC: bouton: 2.3 ± 0.1 ms; axon: 3.7 ± 0.2 ms, $n = 6$, $p < 0.001$, paired t-test). Data are presented as mean ± SEM. *$p < 0.05$, ***$p < 0.001$, n.s., not significant.

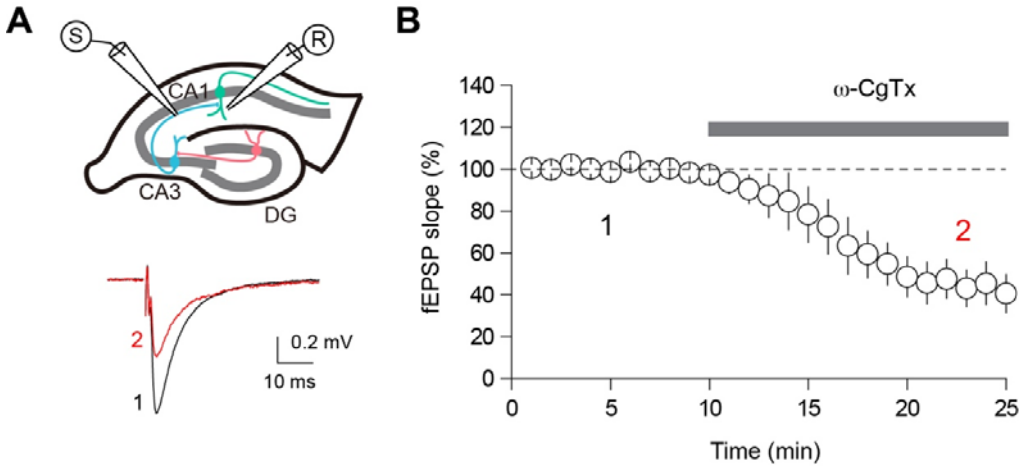

Figure S2. The effect of ω-CgTx on CA3-CA1 transmission (Related to Figure 2)

(**A**) (top) Schematic diagram illustrating the extracellular field excitatory postsynaptic potential recording (fEPSP) configuration. Both the recording and stimulating electrodes were placed in the stratum radiatum of CA1. (bottom) Representative fEPSP traces before (black) and after (red) application of ω-CgTx (500 nM). (**B**) Summary time course plot showing inhibition of CA3-CA1 transmission by ω-CgTx (44.5 ± 9.5% of baseline, $n = 5$, $p < 0.01$, paired t-test). Data are presented as mean ± SEM.

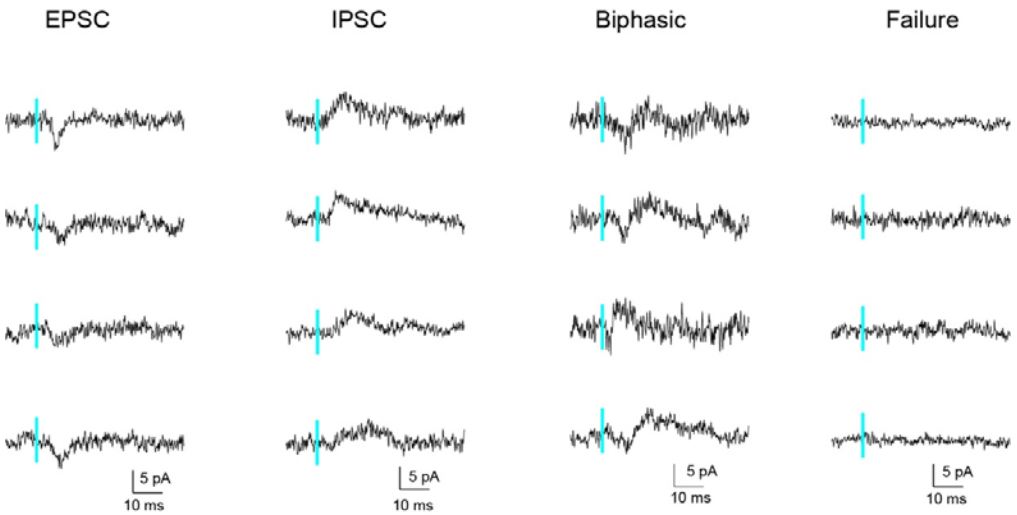

Figure S3. Minimal light stimulation-evoked synaptic responses at SuM-GC synapses (Related to Figure 3)

Sample traces recorded from GCs at holding potential of -20 to -30 mV in response to minimal light stimulation.

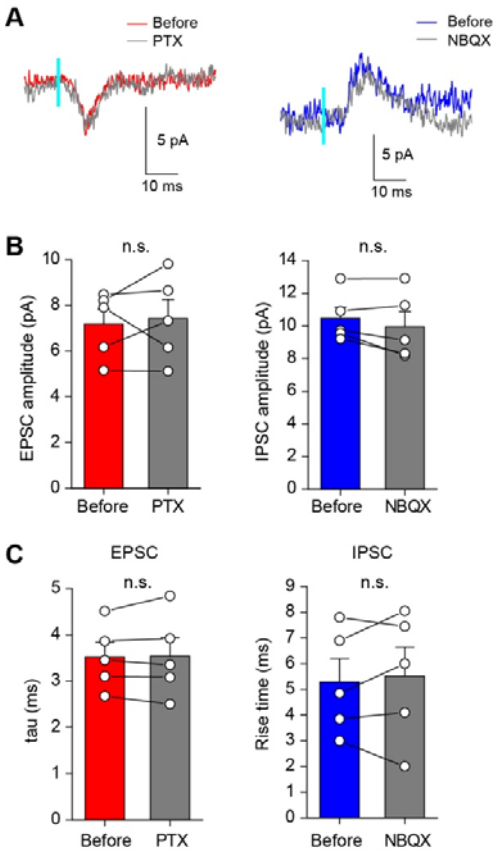

Figure S4. The amplitudes and kinetics of minimal light stimulation-evoked EPSCs or IPSCs at SuM-GC synapses were not altered by blockade of their counterpart currents (Related to Figure 3)

(A) Representative traces of EPSCs (left) and IPSCs (right) evoked by minimal light stimulation of SuM inputs at intermediate membrane potentials. EPSCs or IPSCs were recorded by repeating the light stimulation 100 times before, with the application of 100 μM picrotoxin (PTX) or 10 μM NBQX, respectively. **(B)** Summary plots show that the amplitudes of EPSCs and IPSCs were not changed after application of picrotoxin or NBQX, respectively (EPSC: before: 7.2 ± 0.6 pA; PTX: 7.4 ± 0.8 pA, n = 5, p = 0.71, paired t test; IPSC: before: 10.5 ± 0.7 pA; NBQX: 10.0 ± 0.9 pA, n = 5, p = 0.18, paired t test). **(C)** Summary plots of the decay time constant of EPSCs (tau, single-exponential fit) and rise time of IPSCs (10%-90% of IPSC peak amplitude) (tau: before: 3.5 ± 0.3 ms; PTX: 3.5 ± 0.4 ms, n = 5, p = 0.84, paired t test; rise time: before: 5.3 ± 0.9 ms; NBQX: 5.5 ± 1.1 ms, n = 5, p = 0.60, paired t test). Data are presented as mean ± SEM. n.s., not significant.

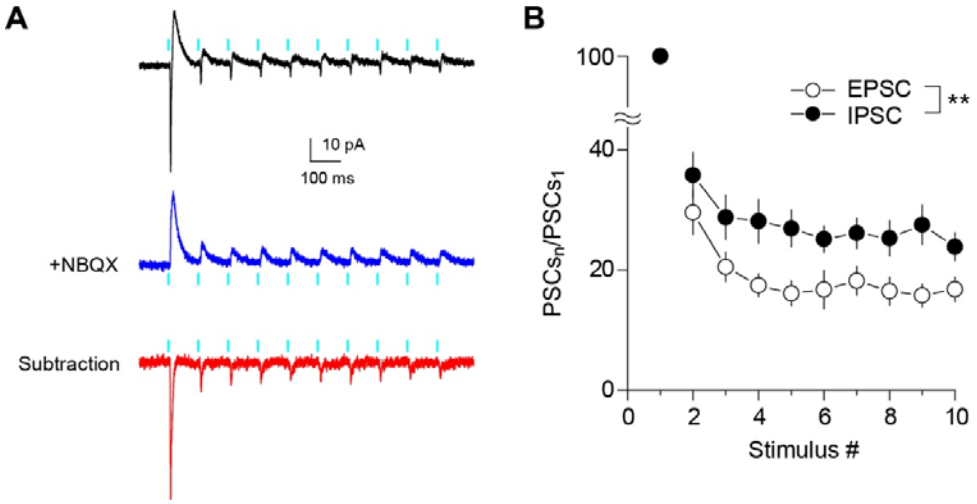

Figure S5. Short-term changes in EPSC/IPSC ratio during train stimulation at SuM-GC synapses (Related to Figure 5)

(**A**) Representative PSCs in response to 10 light pulses at 10 Hz recorded from GC at holding potentials of -30 mV before (black) and after application of 10 μM NBQX (blue). The EPSC (red) was isolated by subtracting the blue trace from the black trace. 1 μM TTX, 500 μM 4-AP, 50 μM D-AP5, 100 μM LY341495, and 3 μM CGP55845 were included in the extracellular solution throughout the experiments. (**B**) Summary graph of normalized EPSC and IPSC amplitudes plotted against stimulus number. Two-way repeated measures ANOVA, $F_{(1,7)} = 17.5$, $p < 0.01$, $n = 8$. Data are presented as mean ± SEM. **$p < 0.01$.

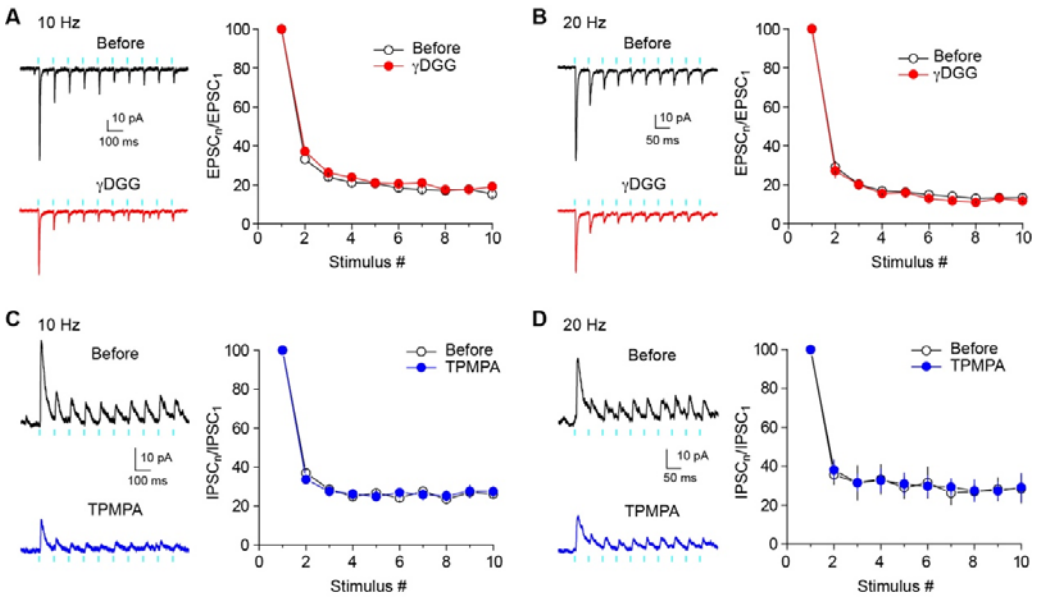

Figure S6. Preventing postsynaptic saturation and desensitization does not alter short-term depression of EPSCs and IPSCs (Related to Figure 5)

(**A and B**) (left) Representative traces showing EPSCs in response to 10 Hz (A) or 20 Hz (B) light stimulation before (top) and after (bottom) application of 2 mM γDGG. (right) Summary graph of normalized EPSC amplitudes plotted against stimulus number. 10 Hz: Two-way repeated measures ANOVA, $F_{(1,7)} = 1.78$, $p = 0.22$, $n = 8$. 20 Hz: Two-way repeated measures ANOVA, $F_{(1,7)} = 0.65$, $p = 0.45$, $n = 8$. (**C and D**) (left) Representative traces showing IPSCs in response to 10 Hz (C) or 20 Hz (D) light stimulation before (top) and after (bottom) application of 300 μM TPMPA. (right) Summary graph of normalized IPSC amplitudes plotted against stimulus number. 10 Hz: Two-way repeated measures ANOVA, $F_{(1,5)} = 1.02$, $p = 0.44$, $n = 6$. 20 Hz: Two-way repeated measures ANOVA, $F_{(1,4)} = 0.21$, $p = 0.67$, $n = 5$. Data are presented as mean ± SEM.

Table S1. List of primary antibodies used in the present study.

Molecules	Sequence (NCBI #)	Host	RRID	Specificity	Source	Figure
$GABA_A\gamma2$		Rb	AB_2263066	KD	Synaptic Systems (224003)	Fig. 4
GluN1		Ms	AB_2571605		Millipore (MAB363)	Fig. 4
VGluT2	559–582 aa (BC038375)	Gp	AB_2571621	IB	Miyazaki et al., 2003 (MSFR107440)	Fig. 4
		Go	AB_2571620	IB	Kawamura et al., 2006 (MSFR106270)	Fig. 4
		Rb	AB_2571619	IB	Miyazaki et al., 2003 (MSFR106300)	Fig. 1
VGAT/VIAAT	31–112 aa (BC052020)	Rb	AB_2571622	IB	Miura et al., 2006 (MSFR106120)	Fig. 4
		Gp	AB_2571624	IB	Miura et al., 2006 (MSFR106150)	Fig.1, 4
GFP		Go	AB_305643		Abcam (ab6673)	Fig.1